THE INFLUENCE OF SURFACE ROUGHNESS AND HUMIDITY ON GLASS-GLASS AND GLASS-STEEL FRICTION

BY

JOHN STEELE ABBOTT

A THESIS
SUBMITTED TO THE FACULTY OF

ALFRED UNIVERSITY

IN PARTIAL FULFILLMENT OF THE REQUIREMENTS
FOR THE DEGREE OF

MASTER OF SCIENCE

IN

MATERIALS SCIENCE AND ENGINEERING

ALFRED, NEW YORK

FEBRUARY, 2019

THE INFLUENCE OF SURFACE ROUGHNESS AND HUMIDITY ON GLASS-GLASS AND GLASS-STEEL FRICTION

BY

JOHN STEELE ABBOTT

B.S. THE JOHNS HOPKINS UNIVERSITY (2005)

SIGNATURE OF AUTHOR_____

APPROVED BY_____

DR. WILLIAM LACOURSE, ADVISOR

_____

DR. WILLIAM CARTY, ADVISORY COMMITTEE

_____

DR. HOLLY SHULMAN, ADVISORY COMMITTEE

_____

DR. JUNJUN DING, CHAIR, ORAL THESIS DEFENSE

ACCEPTED BY_____

GABRIELLE G. GAUSTAD, DEAN
KAZUO INAMORI SCHOOL OF ENGINEERING

ACKNOWLEDGEMENTS

This was quite the journey. When I finished my undergraduate studies many years ago, I mistakenly thought I was done with school. When I embarked upon the path of seeking my Masters degree while working full-time the better part of a decade later, I started along this path without really understanding what I was getting into. There were many occasions where quitting would have been the easier choice, and there were a couple instances where that was closer to happening than anyone will ever know. But it didn't, thanks to everyone who offered their help and support along the way.

Mom and Dad, for their constant support and gentle nudging to keep me moving forward.

Dr. LaCourse, for his support and patience as my advisor, and his willingness to work with someone who was not always the most conventional student.

Dr. Carty and Dr. Shulman, whose questions and ideas helped me think more critically about my work and spurred thoughts about other interesting areas adjacent to this work that might merit investigation.

Doug McElheny, who helped me secure many of the resources I needed to complete this work, and whose support was one of the biggest reasons that I successfully completed this thesis.

Ji Wang and Matthew Abrams, who graciously offered their input and acted as sounding boards for my ideas during the early phase of this work.

Tonia Fletcher, who helped me secure lab space in which I performed much of this work, and offered encouragement as well as insights on the process of doing graduate school while working full-time as an engineer.

Max Bliss, Mike Collier, and Brian Stutts, for their support in allowing me to pursue my degree while working full time.

Casey Volino, whose influence inspired me to improve my data analysis skills, and without whom I would not be the engineer I am today.

And everyone else who stuck with me over the course of this journey. Thank you, everyone.

TABLE OF CONTENTS

Page

LIST OF TABLES

Page

LIST OF FIGURES

Page

ABSTRACT

Effects of environment, and surface roughness on the frictional behavior of aluminosilicate, borosilicate, and soda-lime glasses in contact with glass and 304 stainless steel substrates were tested. Glass and stainless steel substrates produced distinctly different frictional behavior, particularly in dry and humid environments. All dry interactions except for roughened glass-on-glass exhibited a significant increase in mean friction relative to measurements at ambient humidity; this effect was most prominent on stainless steel substrates, and grew progressively stronger for smoother stainless steel substrates.

There was a distinct interactive effect between the roughness of the system and its frictional behavior at elevated humidity For all test conditions where at least one substrate was substantially rough, there was little or no change in friction from ambient humidity to humid conditions, while smooth-on-smooth interactions exhibited substantial increases. This can be attributed to the adhesive contribution of adsorbed surface water films at elevated humidity; the thickness of these adsorbed films relative to the surface topography of the samples is critical to this interaction.

Surface roughness was an important factor in frictional response, but conventional surface roughness metrics such as R_a and rms values were insufficient to define the difference between “smooth” and “rough” surfaces, as electropolished stainless steel behaved in a manner more consistent with smooth surfaces, despite its relatively large roughness values over the length scales employed for the surface roughness measurements. This can be attributed to the fact that electropolishing produces a very smooth surface over short length scales that is not completely quantified by conventional roughness measurements, and that this process produces broader, smoother asperities with a larger effective radius, thereby increasing effective contact area and adhesion effects.

Results can be explained by the dual roles of water in frictional processes, as both a chemical facilitator of hydrolysis for bonds under mechanical strain, and as a film creating adhesion between two contacting surfaces.

I. INTRODUCTION

Glass is employed in numerous industries due to its combination of physical, chemical, and optical properties. Its physical rigidity, resilience in a wide range of environments, and optical clarity make it a material of choice for a diverse range of applications including flat-panel displays, beverage containers, cookware, architecture, and automotive applications. In virtually all instances the mechanical integrity of the glass article is important for the product. In many of these applications, the optical purity of the glass surface is also an important consideration. Any visible scratching, marring, or material transfer to the glass surface is a cosmetic defect, and surface damage has the potential to reduce the strength of the glass. Hence, design of manufacturing processes that handle glass without inflicting such damage is critical to the commercial production of glass.

During glass processing and subsequent handling, it is inevitable that glass parts will contact other materials, and potentially other glass parts. This contact may take many forms, including blunt or sharp impacts, pressure leading to flexion, or friction. The occurrence of significant impact events is often readily observable, and is frequently well-diagnosed and designed out of systems. By comparison, frictional contact may be more subtle. Frictional events may be brief and non-obvious, but they can still create substantial mechanical and optical defects. Furthermore, frictional contact is nearly impossible to avoid completely: short of suspending parts on an air bearing, glass must be contacted by another solid surface in some manner during many processing steps, and the pertinent question becomes not of whether the glass will encounter friction with another material, but rather a question of the location of the frictional contact on the glass article and the severity of the forces involved. For most applications the approach to this problem is straightforward: first, restrict contact to the glass to a limited area, and to one of minimal optical and mechanical concern; second, optimize material properties: select a material with a hardness lower than the glass and/or one with which glass has a low coefficient of friction, thereby minimizing the potential for glass damage from a frictional event.

While a broad range of materials can be utilized for glass handling in mild environments at lower temperatures, much glass processing occurs at high temperatures and/or aggressive environments that severely constrain material selection. For example, annealing processes require parts to be stabilized while traveling through an oven at temperatures potentially exceeding 600C; chemical strengthening processes not only involve process temperatures exceeding 400C, but the glass and its fixturing are immersed in molten nitrate salts, thereby subjecting materials to an exceptionally oxidative environment; cost-effective materials capable of surviving repeated cycles in these environments are a relatively small set: stainless steels, ceramics, and glasses are the most common materials that will survive these harsh environments with their properties largely intact. Even if there is no relative motion during the process when the parts are hot, the parts must still be loaded into and unloaded from fixturing before and after these processes, events which run a high risk of frictional contact. Due to these constraints, the potential for materials to inflict strength-limiting flaws against glass parts via frictional mechanisms is a significant concern in the design of high-temperature glass process equipment.

This work examines factors influencing the coefficient of friction between a glass specimen and another surface, particularly as a function of the material comprising the other surface, the roughness of the surfaces involved in the frictional event, and the humidity under which the friction occurs. This experimentation was done with the implication that coefficient of friction is a useful measure of the forces exerted on a glass specimen during interaction with another surface, and that it is situationally predictive of the surface damage and/or material transfer experienced by the glass article during such an interaction.

The methodology employed in this study utilizes dynamic coefficient of friction measurements while varying factors with the potential to influence frictional behavior against glass to assess their impacts. Dynamic friction measurements were chosen due to the advantages they afford over static measurements. While static frictional measurements are widely used and easily accessible via devices such as an inclined plane tester, such measurements also have several critical limitations. The most significant difference is that there is much less data in a single static coefficient of friction

measurement when compared to a dynamic friction measurement. Static friction data is comprised of a single point corresponding to a specific contact event, whereas dynamic friction measurements enable analysis of a larger area over an extended duration. Thus a "single" dynamic friction measurement effectively incorporates a much larger data set, and is capable of interrogating phenomena that static friction measurements cannot, such as wear effects and stick-slip behavior. Dynamic friction measurement thus produces a much more powerful data set for analysis, although it requires a more complex setup to obtain these measurements, more sophisticated data processing and analysis, and it presents the additional challenge of understanding effects that might influence not just sample-to-sample variability, but temporal and spatial variability within a single sample.

II. LITERATURE SURVEY AND BACKGROUND

A. Friction Theory and its Origins

The fundamental relationships governing friction are often referred to as "Amontons' law(s)", named for the 17th/18th century scientist Guillaume Amontons. However, the origin of these theories predates Amontons' work, and the earliest theoretical discussion of friction has been attributed to Leonardo Da Vinci.[1] These two foundational components of macroscopic friction theory attributed to Da Vinci, and later Amontons are:

1. The frictional force between 2 bodies is independent of the (apparent) area of contact between those two bodies.
2. The frictional force between two bodies is proportional to the normal force between them.[2]

Coulomb further expanded upon this, specifying that for sliding friction, the magnitude of the frictional force is independent of the sliding velocity.[1] Combined, these "laws" comprise the traditional friction equation, which is widely accepted as a first-order approximation and a reasonable starting assumption for predicting friction mechanics over a wide range of situations:[2]

$$F_f = \mu F_n \qquad (1)$$

While this empirical relationship has been recognized for centuries, hypotheses around the underlying mechanisms have continually evolved over time, as the advent of progressively more sophisticated friction testing techniques and improved surface interrogation methods enabled a more refined understanding of the precise phenomena governing friction.

Coulomb was also the earliest to propose one of the other foundational concepts of modern friction theory - that friction between materials was driven by interaction of microscopic surface features known as asperities, one contributor to the broad category of surface attributes that humans may perceive as roughness. Coulomb hypothesized that friction was a function of the geometry of these asperities, with a mechanism like the

effect of pushing an object up a hill. In principle, pushing an object up of mass *m* up a hill with slope θ should require a horizontal force of *m* tan θ, and hence coefficient of friction of tan θ.[3] Tabor notes that there are multiple fundamental problems with this hypothesis: first, this mechanism does not account for the dissipation of energy in a frictional process, and second, unknown during Coulomb's time due to lack of sophisticated profilometry, typical surface asperities have a relatively shallow angle of 5 to 10 degrees, resulting in a theoretical value of 0.09 to 0.18 for the tan θ term. Considering that the measured coefficients of friction can greatly exceed these values, it is evident that while this term may be relevant and nontrivial, it cannot possibly comprise the majority of frictional force for materials with high coefficients of friction.[3]

The influence of asperity slopes on frictional mechanics is still widely discussed in literature, although they are no longer regarded as the primary driver of frictional mechanics. Ludema notes that multiple authors have proposed equations of the form:

$$\mu = \frac{S_x}{P_y} + tan\,\theta^4 \qquad (2)$$

Tabor references the value $2/\pi$ * cot θ, where θ is the complement of the angle that Ludema references.[3] In this case, tan θ is a "plowing" term where θ is the angle of surface asperities. This equation represents an empirical fit of observed data, and does not address the fundamental mechanisms governing friction on the microscopic scale.

As analytical methods have improved, modern friction theory has gravitated toward the concept of adhesion – the product of the attractive forces that exist between two surfaces in proximity. While there are multiple components to these attractive forces, they are governed by the laws of thermodynamics: the sum of forces on a stationary object is zero by definition, and a system will seek out the most stable, lowest-energy thermodynamic state. Among the forces manifesting as components of adhesion/friction are intermolecular/attractive forces including van der Waals forces and surface charge effects. Additionally, surface tension forces associated with thin films of adsorbed water on the surface of solids in humid environments can contribute substantially to adhesion/friction depending on the surface energy of the materials in question.[3] These phenomena have been interrogated by several techniques, including examination of adhesive forces via AFM[5] as well as comparing friction/adhesion with

surface charge by conducting zeta potential measurements along with friction testing in varied environments.[6] Alteration of any of the component contributors to adhesion will affect the total adhesion, and hence the friction between two surfaces.

B. Contact Theory and Adhesion

Modern friction theory holds that adhesion and friction are functions of the true contact area between two surfaces. Multiple models have been developed to attempt to simulate and predict the effects of these mechanics, ranging from simple elastic contact to plastic contact, and ultimately incorporating adhesive contributions to provide comprehensive models of contact mechanics. Additionally, multiple methods have been used to incorporate the potential variation in geometry among surface asperities into these models.

As referenced by Johnson,[7] the earliest attempt to mathematically define the area of contact between two bodies was by Heinrich Hertz, for whom the foundational contact theory is named. Using a spherical approximation for asperity shapes and neglecting adhesive mechanisms, Hertzian theory predicts that for elastic contacts, the area of contact would scale proportionately to the applied load to the $2/3^{rd}$ power. However, as Persson points out, this is inconsistent with many bodies of experimental data, which exhibit a more linear proportionality between applied load and frictional force. An alternative model was proposed by Greenwood and Williamson: they treated the surface as a set of spherical asperities and employed a Gaussian height distribution to more accurately represent the surfaces of real materials.[8] Greenwood and Williamson's work predicts an outcome very close to the linear relationship between normal and frictional force predicted classical friction theory, as real contact area and hence friction were roughly proportional to the applied load.[9]

An even more comprehensive theory of surface roughness and contact was developed by Bush, Gibson, and Thomas. The defining element of this theory is that there are not merely one or two relevant length scales when considering asperity size distributions, but many.[8] This model also agrees very well with the typical experimental observations of friction proportional to applied load, with the effective coefficient of

friction in this model depending only on the Hertzian elastic modulus and the mean slope of surface asperities.[10]

Further evolution of contact models incorporated the addition of adhesive mechanisms between surfaces. While non-adhesive models may be reasonably accurate in situations where applied normal forces are large and/or normal adhesive forces are small by comparison, many frictional phenomena involve adhesive forces comparable to or even exceeding applied normal forces. One of the foundational models for adhesive contact is the contact model developed by Johnson, Kendall, and Roberts, commonly referred to as the JKR model. The crucial, foundational aspect of the JKR theory is the incorporation of surface energy and the resulting adhesive force in predicting the area of contact between two elastic solid surfaces. The work of JKR showed that while Hertzian theory predicted contact behavior accurately in environments where surface energy was low/negligible, the incorporation of surface energy into calculations produced a model that reflected experimental results much more accurately in environments where surface energy and adhesion were significant.[11] Fuller and Tabor expanded upon this work and incorporated JKR theory with the asperity model of Greenwood and Williamson to produce a comprehensive model that is an effective predictor of contact and friction over a wide range of conditions.[8]

It should be noted that these models explicitly deal with elastic deformation and adhesive processes; with plastic deformation or junction growth that may occur when local stresses exceed a ductile material's yield stress this may not be the case. Hence these models are effective for predicting friction and adhesion for a single event, but are relatively ineffective at dealing with plastic deformation or wear events.

C. Heat Treatment and Surface Preparation

When evaluating the mechanical properties of a glass surface, it is crucial to understand what is truly being measured. While a friction measurement may appear to be occurring on a glass surface, in practice it could be influenced by wear particles or environmental contaminants on that surface. Furthermore, methods used to remove surface contaminants may potentially alter the glass surface as well, thereby necessitating

a thorough understanding of the phenomena associated with any surface preparation technique. Heat treatment is one of the simplest and safest techniques for preparing glass surfaces for other treatments and is highly effective at removing organic contaminants that may influence the frictional behavior of glass.

Surface energy is a measure of the reactivity of a surface: Compared with lower-energy surfaces, high-energy surfaces possess a greater quantity of chemically-active groups with the potential to form bonds or otherwise interact with other surfaces. Thus, these surfaces require a greater quantity of bond formation/material interactions to reach thermodynamic equilibrium. One way surface energy can be assessed is via contact angle with water: higher-energy surfaces exhibit a lower contact angle with water, as a water droplet must spread out and interact with a greater number of hydroxyl groups on the glass surface before equilibrium is reached with the water's surface tension.[12] This increased surface reactivity can also manifest as a greater number of bonds between the high-energy surface and another material before equilibrium is reached. It naturally follows then, that a more energetic surface has the potential to exhibit greater adhesive force when contacted by another object when compared with a nonreactive surface.

Several noteworthy studies have looked at the impact of heat treatment cycles on glass surfaces, focusing on the effects of time and temperature:

Butz examined the effects of glass heat treatment cycles on both static coefficient of friction and contact angle, observing that there was a decrease in contact angle and an increase in static coefficient of friction associated with longer and hotter thermal treatment cycles. In practice, static coefficient of friction reached a maximum of approximately 0.7 after a heat treatment cycle of 60 minutes at 300C. Contact angle reached a minimum of approximately five degrees with the same cycle. Cycles that were longer or hotter did not substantially decrease the measured coefficient of friction beyond this level.[13]

Similarly, Jenkins found that the coefficient of friction for soda-lime silicate glass plateaued at approximately 1.0 after a 15-minute thermal cycle at 350C. Critically, Jenkins also found that heat treatments of 300C or below did not reach the same maximum coefficient of friction, and that longer, hotter heat treatments of 450C at anywhere from two to sixteen hours exhibited a gradual decrease from the initial friction

maximum.[14] This is consistent with the rapid removal of organics at a sufficient heat treatment temperature, followed changes to the surface of the glass and relaxation of strained bonds over much longer time scales. The latter observation is also consistent with the observations of this author that extreme thermal treatments for durations of 48 hours or more at temperatures exceeding 350C can significantly reduce the surface energy of glasses as characterized by contact angles as high as 30 to 50 degrees.[15]

During thermal treatment, adsorbed water and hydroxyl groups are removed from the surface of glass; after the completion of a thermal treatment cycle, the glass surface gradually recovers this lost surface moisture. D'Souza and Pantano examined dehydration and rehydration kinetics of silica samples as a function of heat-treatment cycle heat-treated at 350C for 20 hours returned to near their initial hydration state in under 15 minutes; Samples heat-treated at 500C lost more hydroxyl groups and did not recover as rapidly, or completely upon return to a cooler, more humid atmosphere. This effect became even more pronounced as heat treatment durations lengthened.[16] The authors attributed this to the relaxation phenomena that can occur at long times at elevated temperatures as well as the removal of bonds/hydroxyl groups that are normally stable at lower temperatures but reform much more slowly when lost, resulting in a less-energetic surface with fewer free hydroxyl groups.

D. Humidity and Friction

Water plays a critical role in frictional mechanics for a wide range of materials. Contrary to the layperson's perception that surface moisture is only present in condensing environments, in all but the driest environments there is some quantity of adsorbed water on the surfaces of materials; the thickness of this film is dependent on the material and humidity. This film plays a crucial role in a wide range of material properties dependent on a material's surface condition.

Several authors have investigated the nature of water adsorption to glass surfaces. Asay and Kim describe the nature of adsorbed water on silica surfaces and its evolution with increasing humidity. The first few layers of adsorbed water are "ice-like" – hydrogen – bonded and orderly, like the crystalline structure of ice. At less than 30%

relative humidity there may an ice-like layer of water up to 3 molecules thick on the surface of the silica; at high humidity levels a thicker, truly liquid film of water begins to build on top of this layer. Critically, Asay and Kim note that this ice-like layer has a greater surface tension than a typical water film due to its greater extent of hydrogen bonding. Thus, this ice-like layer could result in greater adhesive forces for a given true contact area than a typical water film.[17]

Stainless steel will similarly acquire an adsorbed water film in all but the driest environments. Subhi, Fukuda, Morita, and Sugimura found that the thickness of the adsorbed water film on a 316 Stainless Steel surface ranges from <1 nm at 3% relative humidity to ~30 nm at moderate humidity, to as much as 60 nm near saturation. Most of this increase in surface water occurred over the range of 3% to 65% relative humidity.[18]

McFarlane and Tabor examined the role of humidity on glass, focusing particularly on its behavior in humid environments. They cite the work of McHaffie and Lenher[19] where glass surfaces have no more than a few layers of water at less than 50% relative humidity, up to 100 layers or greater as humidity levels approach saturation. They also describe a progressive decrease in measured adhesion in saturated humidity environments as glass is progressively roughened, to effectively zero for specimens with surface features approaching 10 microns in height. The authors inferred that this sharp drop in adhesion occurred because the height of asperities on the glass surface exceeded the thickness of the adsorbed liquid film, thereby decreasing the effective contact area of the water film and hence its contribution to adhesive forces.[20]

He, Qian, Pantano, and Kim studied the effect of humidity on friction between a soda-lime glass substrate and a stainless steel stylus as a function of humidity; At a very low number of cycles, friction was highest for low-humidity conditions; after large numbers of cycles friction was highest at elevated humidity.[21] In a separate paper, the same group looked at glass-glass contact; after a small number of cycles the coefficient of friction was highest for both the dry and humid conditions; after extended cycling the most humid conditions exhibited the highest coefficients of friction. Notably, at low to moderate humidity material transfer from the soda-lime substrate to the borosilicate glass ball was observed, while at high humidity there was significant wear of the borosilicate ball.[22]

Jones and Pollock found via AFM studies that glass-to-glass adhesion increased progressively with increasing humidity. They also observed that 100-micron glass spheres exhibited significantly lower adhesion at all humidity levels than 20-micron glass spheres; they observed that these spheres had substantially larger asperities than the smaller spheres, and attributed this as a possible cause.[5]

E. Wear/Surface Effects and Friction

Wear plays a critical role in any frictional process over time, regardless of the materials involved. During frictional processes, bond breakage occurs at the weakest component of the system; depending on the materials and environment this can take the form of fracture, ductile transformation, material removal, or slipping/lubricated motion at a fluid interface between two surfaces. In nearly all cases there will be a significant change in surface condition over time, and in many cases material will transfer from one surface to the other, resulting in a different set of surface interactions than that between two pristine surfaces. Alternatively, brittle fracture or material removal may occur such that the two surfaces ride on a layer of wear particles from one or both surfaces rather than the original surface interaction. Furthermore, ductile materials can deform, resulting in alteration of asperity shapes and enlargement of potential contact area, or oxide films can be altered or removed entirely, thereby altering a material's surface chemistry.[23] In all instances it is critical that the experimenter understand how the surfaces being tested evolve over the course of testing.

He, Qian, Pantano, Kim demonstrated that for glass-steel contact, initial friction is highest for samples tested under dry conditions and lowest for samples in humid environments. However, after extended testing the highest friction occurs at moderate humidity levels. This is due to differing wear mechanics as a function of humidity. At low humidity material transferred from soda-lime substrates to a stainless steel ball over time; at higher humidity the stainless steel surface itself suffered erosion but there was little wear on the glass substrate.[21]

For metallic materials capable of plastic deformation rather than brittle fracture, the potential for this mechanism to influence contact mechanics is of particular

importance when considering frictional behavior. This deformation will occur when the local stress on a material exceeds the material's yield stress, and asperities will flatten out under the shear, increasing the effective contact area between surfaces. As friction continues, this process may eventually be negated by debris generation, resulting in a roughening of the effective surface topography.[23] This is consistent with the work of Godfrey and Bailey, who tested friction between glass and copper, and observed that friction initially rose from 1.2 to 1.6 before gradually declining to a value near 0.5. This was accompanied by some transfer of copper material to the glass, and the formation of an oxide film on the copper.[24]

F. Roughness, Friction/Adhesion, and Wear

Modern friction theory holds that friction is primarily determined by the area of contact between two surfaces, and the adhesive forces in that region as a function of the materials involved. As such, numerous studies have examined the relationship between surface roughness, asperity heights, and frictional behavior of materials.

Bhusan, Koch, and Jung demonstrated that adhesion reached a minimum when a microstructured surface was surfaces was roughened to the nanometer scale. This was accompanied by an increase in contact angle. The authors attributed this behavior to the propensity for the nanostructured surface to form and retain air pockets on the nanoscale, decreasing the effective contact area of adsorbed liquid films, and hence lowering the contribution of surface tension of liquid films to adhesion.[25]

Jones, Pollock, and Cleaver note that the scale of Kelvin meniscus radii of water relative to asperity dimensions is a significant factor in capillary bridging in surface films, and indeed, the results of their work were consistent with this. They suggested that the relative thickness of adsorbed water films versus surface roughness/asperity size was one explanation for why there was a large discrepancy between the adhesion-humidity relationships for two different glass balls with differing degrees of surface roughness, as well as for much of the divergence between their experimental adhesion measurements and theoretical calculations of adhesive force for the conditions tested.[5]

Tabor found that under humid conditions, the measured adhesion between two surfaces had an inverse relationship with surface roughness, with the adhesive contribution from the adsorbed water film decreasing and eventually disappearing as surface roughness significantly exceeded the thickness of the adsorbed water film.[20] Tabor also found that coefficients of friction and adhesion were tightly correlated, strongly implying that adhesion changes due to surface tension effects would likely translate into changes in frictional force.[26]

Belkhir, Aliouane, and Bouzid demonstrated a strong correlation between contact area and friction during glass polishing: As the rough surface became smoother during the polishing process, effective contact area and friction both increased; as the surface was further polished, friction began to gradually decrease. Profilometry demonstrated initial polishing smoothed the surface over short distance scales and enabled a greater effective area of contact. However, the polishing process eventually removed enough material to impart a subtle curvature to the sample surface, thereby decreasing the effective contact angle and the friction between the two surfaces.[27]

Meyer, Fuchs, Staedler, and Jiang observed an unusual relationship in friction between silica surfaces and glass beads: rougher, etched surfaces exhibited a higher initial frictional force, but the friction rapidly declined with time, whereas friction for the smoother, as-received surface remained the same or increased slightly with wear. The authors proposed that this could have been due to plastic deformation of asperities and a change in the real contact area between the samples over time as a function of surface roughness. The same work also found that smooth samples had a nonlinear relationship between normal force and coefficient of friction, while samples that were etched to increase their surface roughness exhibited a more typical linear relationship.[28]

Garzino-Demo and Lama demonstrated significant differences in both initial friction and change in friction as a function of wear for surfaces of varying roughness in tests carried out with a metal pin on a glass substrate. In all cases friction eventually rose from an initial value between 0.4 and 0.6 to a maximum of 1.4 to 1.8, but this shift took substantially longer to occur when testing a rough pin against a smooth glass substrate when compared with smooth metal pins and/or rough glass surfaces. Additionally,

rougher glass substrates exhibited significantly lower frictional variability when compared with smoother glass specimens.[29]

Rahaman, Zhang, Liu, and Liu utilized a similar methodology as Garzino-Demo and Lama, but for explored the effects of two different compositions and two different degrees of roughness for bulk metallic glass pins against a steel substrate. For both glass compositions, the samples had similar friction at the start of the test, but after extensive wear, the rougher pins had a higher overall coefficient of friction. The authors attribute this to both plastic deformation of asperities and material transfer from one surface to the other.[30]

Kalin and Jahanmir found different frictional behaviors for glass-infiltrated alumina on pure alumina as a function of surface roughness: The smoothest samples had an initial coefficient of friction near 0.3 but quickly rose to 0.6 after wear, while the roughest sample started at 0.6 but eventually declined to 0.3. The authors observed a corresponding roughening of the polished sample, and a smoothing of the rougher sample over the course of the testing.[31]

G. Surface finishing of glass and steel

Commercial glasses have exceptionally smooth surfaces, with roughness values on the order of a nanometer or less. This smooth surface is either the product of an untouched surface from the forming process or fine polishing. Float glass has been measured to have roughness values of 0.4-0.6 nm;[32] Fusion-formed glass has similar roughness values as the air side of float glass. Well-polished glass from other forming processes can also approach the nanometer level for surface roughness.

Lapping is a process employed in the commercial finishing of glass, and is typically used when a significant amount of material removal from a glass surface is required. This process has the effect of roughening the glass surface, and is typically followed by a fine polishing process to restore the glass surface to a smooth, optically clear state. Hard abrasive media such as SiC or Al_2O_3 is commonly used in lapping processes; The rate of material removal and resulting surface roughness are dependent on the media and other process parameters such as applied pressure. Belkhir, Bouzid, and

Herold found that surface roughness of samples lapped by alumina grit ranged from 330 to 1390 nm RMS with grit sizes ranging from 7 to 80 microns.[33]

Most commercial steels have surfaces produced by mechanical contact: either an as-formed surface produced by a rolling process, or a machined surface produced by abrading or polishing the steel with an abrasive agent of the desired grit size. Typical roughness specifications for mechanical steel finishes are on the order of 1 micron for #3 and around 50 nm for #8 finishes,[34] though some finishing processes may yield smoother surfaces than these specifications.

Electropolishing is an alternative process for smoothing the surface of metals. Electropolishing is performed by using flowing an electric current through an electrolyte bath to selectively remove surface material from metal surfaces. This process preferentially removes small, convex surfaces, and thus is highly effective at rounding or removing very small-scale asperities, while having a lesser impact on larger features. The total material removal from electropolishing is a function of the electrical current and duration of the electropolishing process.[35]

III. EXPERIMENTAL PROCEDURES

A. Conditions/Sample Designations

Below is a summary of labels and naming conventions used in graphs and figures, as well as specifics of the materials and used for testing:

Glass/Steel Specimens:

1. Aluminosilicate (AS): Corning® Gorilla® Glass, not Ion exchanged
2. Borosilicate (Boro): Borosilicate Glass microscope slides
3. Soda-Lime Silicate (SL, SLS): Polished soda-lime float glass
4. Lapped Aluminosilicate (AS-Lapped): Gorilla® Glass, subject to a lapping process to produce a roughened surface
5. #3 Brushed Stainless Steel (SS-3): 304 Stainless steel, with a #3 brushed mechanical finish
6. #8 Mirror-Polished steel (SS-8): 304 Stainless steel, with a #8, mirror-like finish, produced via mechanical polishing
7. Electropolished stainless steel (SS-EP): 304 Stainless steel, electropolished

Humidity Levels:

1. “Dry”: Tested at 10 +/- 5% RH
2. “Ambient”: 40 +/- 5% RH
3. “Humid”: 65 +/- 5% RH

B. Sample Acquisition/Preparation

1. Glass and Stainless Steel Specimens

All stainless steel specimens used in the work were commercially-available stainless steel sheets; all samples were grade 304 steel. #3 “brushed” and #8 “mirror polished” samples were purchased in 6”x6” squares; electropolished samples were

acquired in the form of larger trays that were formed and electropolished at a supplier; these trays were cut to approximately 6”x6” squares for use in testing.

Several commercially-available glass compositions were used in this work. The glass types selected were:

- Aluminosilicate (Corning® Gorilla® Glass, not chemically strengthened)
- Borosilicate glass microscope slides
- Soda-lime silicate float glass, polished

The aluminosilicate and soda-lime specimens were 50 mm x 50 mm; the borosilicate specimens measured 25 mm x 75 mm.

2. Surface Roughening Processes:

Samples were lapped with a standard industrial lapping process: parts were run on a lapping machine using a slurry of 9-micron Al_2O_3 particles with a pressure of 1.5 psi for 5 minutes. After completion of the lapping, the parts were washed in an ultrasonic washer with deionized water to remove any residual material remaining from the lapping process, and dried prior to subsequent processing.

3. Thermal Treatment

Thermal treatment of parts was employed as a means of ensuring a consistent surface condition of parts prior to any coefficient of friction testing. This treatment has the effect of removing organic contamination from the surface of the glass as well as temporarily removing adsorbed water and some fraction of hydroxyl groups from the glass surface. After removal from the thermal process the surface will quickly recover hydroxyl groups and surface water in the presence of atmospheric humidity; re-accumulation of organics occurs over much longer time periods.

For the purposes of sample preparation, both the glass and stainless steel specimens were placed on stainless steel trays and were thermally treated in an oven for a period of one hour at 350C. In subsequent friction testing, only the “up” sides of the

specimens that were not in contact with the tray were tested, to avoid complicating effects from contact with other surfaces during the thermal treatment process. Parts were cooled for a minimum of ten minutes prior to the initiation of friction testing.

C. Coefficient of Friction Testing

The dynamic coefficient of friction tests for this work were executed with a system designed to execute the method detailed in ASTM D1894.[36] This procedure was modified to accommodate the specimens and environmental conditions required for this work. One crucial difference between the procedures defined in ASTM D1894 and this experimental work is that ASTM D1894 specifies a motion rate of 150 +/- 30 mm/min, while all tests for this work were run rate of 50 mm/min. This motion rate was chosen due to the dimensions of the experimental samples and the data acquisition capabilities of the hardware, and permitted the collection of several hundred data points per sample. The primary hardware components of this system were all manufactured by the Mark-10 corporation. The system consisted of an M5-2-COF coefficient of friction gauge containing a 10 N load cell, and a G1086 ASTM D1894 coefficient of friction fixture.

Figure 1. Coefficient of friction test apparatus

The coefficient of friction apparatus consists of a load cell with a force transducer mounted to a motorized stage, with a string that passes around a ball-bearing pulley and attaches to a sled. The mass of the sled is 200 grams, which combined with the typical 4.2-gram mass of the glass specimen, results in a normal force of 2 N +/- 0.5%. For the purposes of experimentation, a stop designed to prevent unintended motion of the stationary bottom specimen was affixed to the horizontal stage with clamps, and the substrate was placed against this stop at the beginning of each test such that no movement was possible. Double-sided tape was used to affix the top glass specimen to the sled. The test was run for forty seconds if specimen dimensions permitted, or the longest feasible test distance for small specimens.

For experimental conditions requiring controlled humidity, the experimental setup was modified to enable environmental control of the test space. The pulley from the mechanical tester was rotated 180 degrees, and the string attached to the sled was threaded through a small hole into an otherwise-sealed plastic box with a volume of approximately 1 cubic foot. Nitrogen or air of the desired humidity was fed to the box at a minimum rate of 4 cubic feet per minute. For the low-humidity samples, the samples were placed in the box and the box was purged with nitrogen until a relative humidity of less than or equal to 10% was achieved. For each subsequent test, the samples were placed in their initial positions, the box was closed, and conditions were equilibrated until the relative humidity inside the box was less than or equal to 12%. For high-humidity conditions, air was bubbled through a series of water-containing vessels to humidify it before feeding into the box. The box was initially purged at the start of each condition until relative humidity reached 65%. For each subsequent test, samples were set up and the box was purged to a minimum of 60% humidity prior to initiation of testing.

Figure 2. Coefficient of friction test setup for high and low-humidity conditions

During the coefficient of friction test, the sled was pulled at a continuous rate of 50 millimeters per minute across the substrate. The gauge was set to acquire data at frequency of 10 data points per second; the gauge was connected to a PC and the data was processed with the MesurLITE software from the Mark-10 corporation, then sent to

Microsoft Excel and saved as a table. Files for each test were subsequently imported via script to JMP statistical software for analysis. For the purposes of analysis, the data was filtered of missing readings due to communication errors or other factors prior to evaluation.

Multiple metrics were calculated from the coefficient of friction data:

1. 2mm average, a measure of the mean coefficient of friction over the previous 2 millimeters/24 points of the test. This metric produces a "smoothed" version of the coefficient of friction plot.
2. 2mm standard deviation, a measure of the standard deviation of the coefficient of friction over the previous 2mm/24 points of the test. This metric is a measure of the amount of short-term "noise" in the friction measurement, and reflects how much friction varies over a short distance. This metric is also sensitive to stick-slip friction events.
3. Overall Average, the overall average coefficient of friction for a given sample.
4. Standard deviation of averages, a measure of the amount of sample-to-sample variability for a particular condition.
5. Inverted distance, the distance from the end of each individual coefficient of friction test. This measure was employed to standardize data sets: It simplifies the elimination of startup effects from the coefficient of friction test where the string is not fully tensioned, and simplifies the equating of data sets by enabling analysis of equal-sized data sets for comparison purposes.
6. Coefficient of Variation(COV): This metric is calculated at the sample level by dividing the standard deviation metric by the mean coefficient of friction for a given sample. This measure is a "normalized" metric of within-sample variability useful for comparison of the various experimental inputs.

Due to the known influence of relative humidity on friction and its criticality as an experimental variable, ambient temperature and humidity in the test room were continuously monitored during experimental work. For the duration of the

experimentation, the ambient test environment was maintained at a relative humidity of 40 +/- 5%, and a temperature of 22 +/- 2C.

D. Contact Angle Measurement

Contact Angle measurements were performed on a Kruss goniometer. The goniometer was operated according to a defined SOP developed to achieve accurate contact angle measurements on a range of glass substrates. The contact angle measurement was performed according to the following procedure:

1. Set the camera focus/calibrate goniometer optics per vendor instructions
2. Lower the dropper needle to near the substrate surface
3. Apply a water droplet with a volume of 1 microliter to the substrate
4. Use the goniometer software to measure the droplet's contact angle
5. Index the sample by 8 mm before applying the next droplet
6. Repeat 5 times per substrate

E. Surface Roughness Measurements

Topographical measurements of specimen surfaces were performed on a Zygo NewView 5000. A minimum of 8 samples were measured for each sample type, and Ra, rms, and PV(peak-valley) values were taken for each sample. These measurements were taken over an area measuring of 0.18 by 0.13 mm. In addition to surface roughness measurements on pristine samples, several wear tracks were examined and the topography of surface alterations was measured on samples after friction testing. For these measurements, the measured area was 1.19 by 5.85 mm.

IV. EXPERIMENTAL RESULTS

A. Surface Roughness

All glass compositions exhibited similar ranges of surface roughness, but substantial differences in the details of the surfaces were evident when the surfaces were examined more closely.

There was evidence of residual material on the Aluminosilicate glass surface, manifested as raised areas often of circular shape. It is likely that this is residue from the film the glass was packaged in that survived the surface preparation process. Comparison of post-treatment samples indicated that peak-valley heights decreased by a factor of 20, and R_a and rms roughness decreased by a factor of 10 relative to untreated samples, suggesting that the thermal treatment process removed most of this residue. However, there is still some evidence of scattered material on the glass surface, suggesting that oxidized remnants of film material remain after the treatment. Given the nature of fully oxidized organic residue, this material likely is brittle and would crumble during a friction event. However, it could still limit glass-to-glass contact area and hence impact frictional force.

The borosilicate glass slides show evidence of local, large asperities, as well as broad areas that are slightly raised or depressed. There is no consistent, observable pattern to the surface topography. The observed material is likely glass transferred from one surface to the next as the samples were separated. These samples were stacked glass-on-glass when they were packaged and spent extensive time in this state, and the material transfer is likely due to strong adhesion between flat samples in close proximity, which led with the difficulty of separating these samples in a consistent manner without material transfer.

The soda-lime glass was polished by the supplier prior to shipment. There were significant differences observed between the two sides of the glass. These differences are most likely the result of differences between the glass and tin sides of a float glass interacting with the subsequent polishing step. By conventional metrics the soda-lime

glass had the smoothest surface of any of the specimens, and had minimal evidence of surface perturbations due to film residues or handling.

The lapped aluminosilicate samples were multiple orders of magnitude rougher than the other glass samples, and had roughness values on the order of 600 nm R_a. The surface roughness of the lapped samples was uniformly across all measurements on all parts, and there was no evidence of local areas or individual specimens that deviated from this significantly.

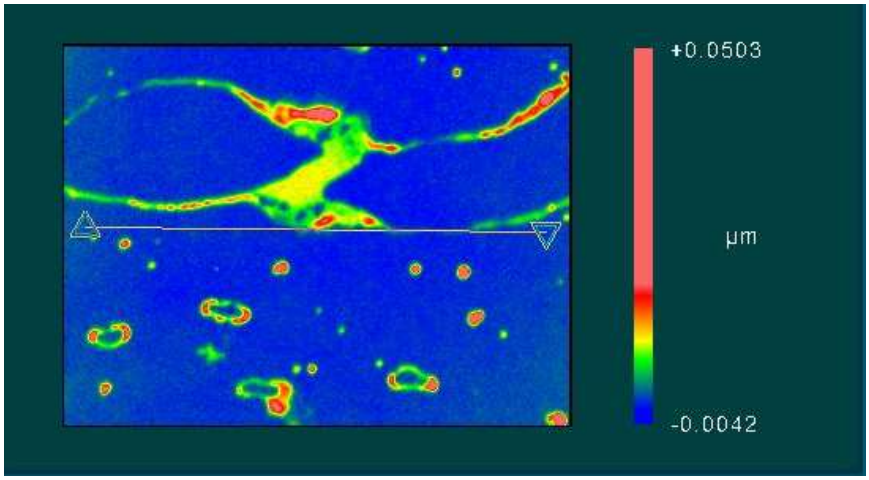

Figure 3. Surface topography of as-received aluminosilicate glass

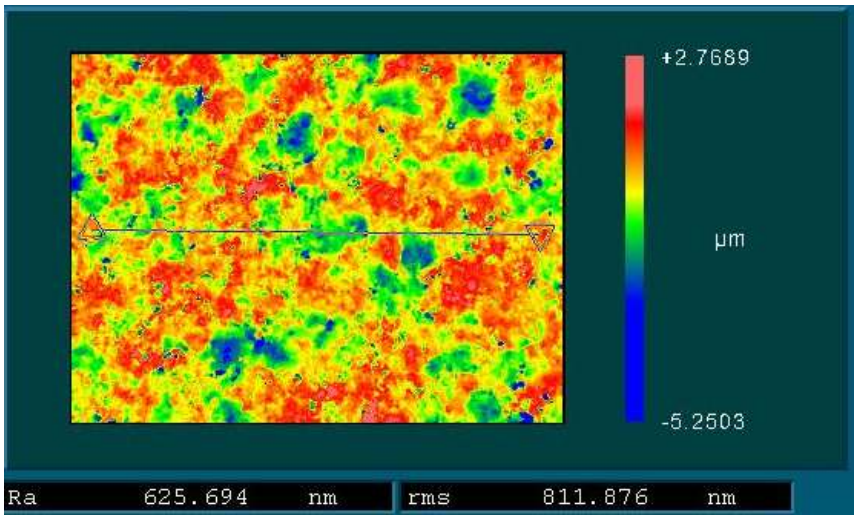

Figure 4. Surface topography of lapped aluminosilicate glass

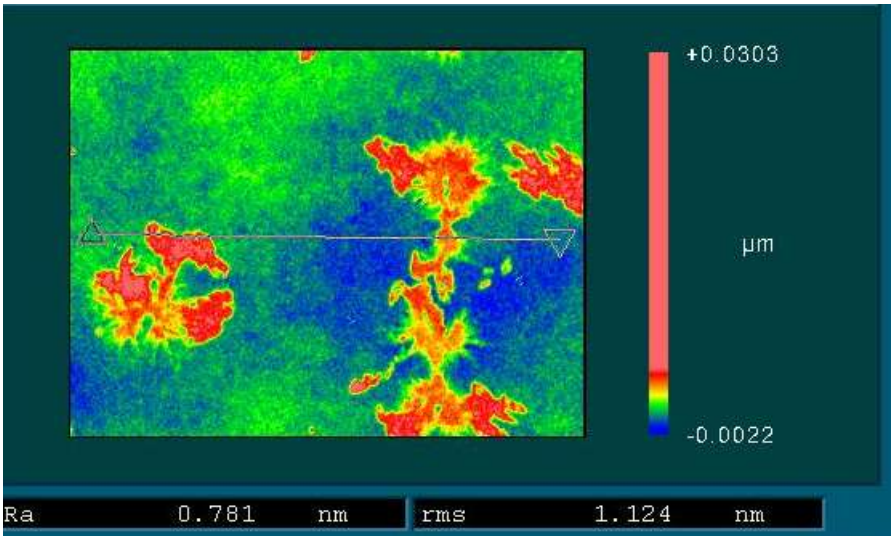

Figure 5. Surface topography of borosilicate glass

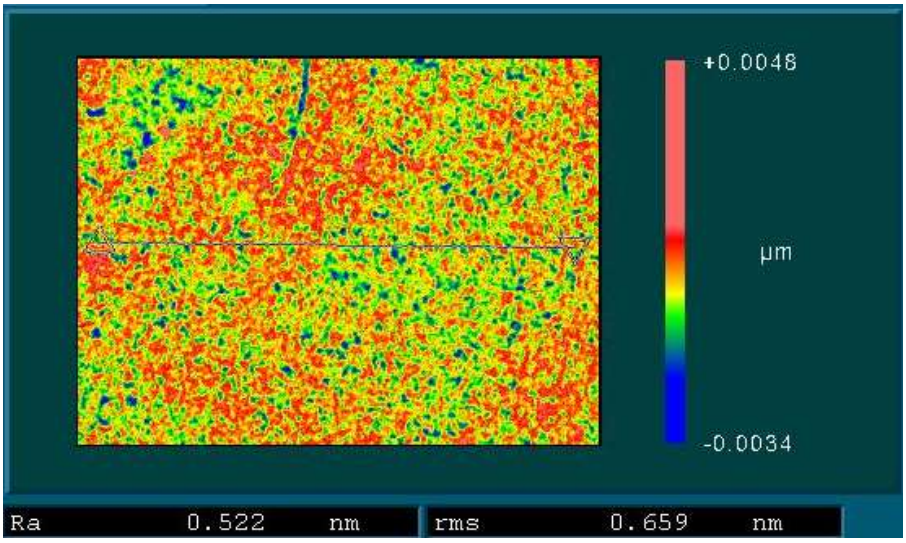

Figure 6. Surface topography of soda-lime glass, "A" side

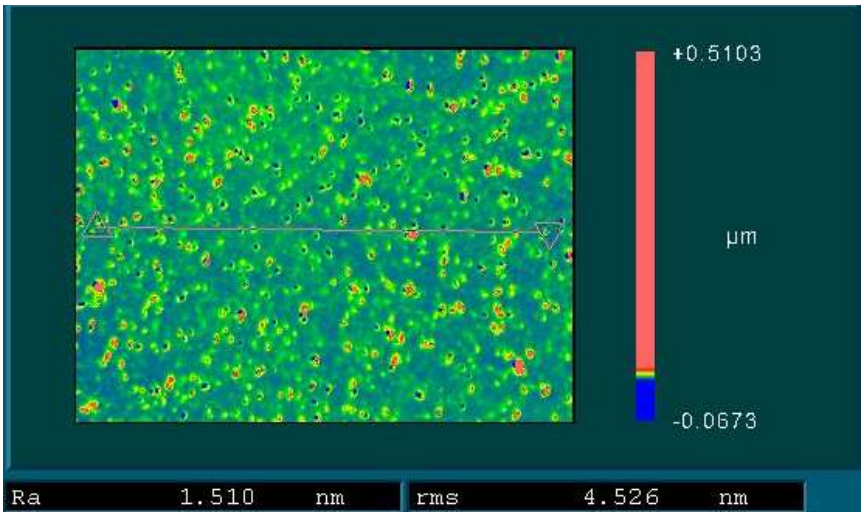

Figure 7. Surface topography of soda-lime glass, "B" side

Both the #3 and #8 stainless steel specimens exhibited a consistent, directional grooved pattern associated with the motion of the mechanical polishing processes used in their manufacture. The roughness of these samples was on the order of several hundred nanometers for the #3 stainless steel, and on the order of 10 nanometers for the #8 stainless steel. It is noteworthy that these values are below the values of 1000 and 50 nm commonly cited for the typical surface roughness of #3 and #8 surface finishes.

The electropolished stainless steel samples used for this experimentation are particularly noteworthy, as they were not adequately described by conventional roughness measures. While the measured surface roughness values for electropolished steel are comparable to those of the #3 stainless steel, it is evident from images of the surface topography that R_a, rms, and PV measurements do not adequately quantify the impact of electropolishing on stainless steel surfaces. While the total peak-to-valley height variation over distances of hundreds of microns or more is comparable to that of mechanically-finished stainless steel, the topography of the profiles illustrates that the electropolished surface is much smoother over length scales on the order of one to ten microns. There is also evidence of small features systematically protruding from the electropolished surface – these may be individual grains from within the stainless steel

material. This appearance is consistent with typical electropolished surface finishes described in literature.

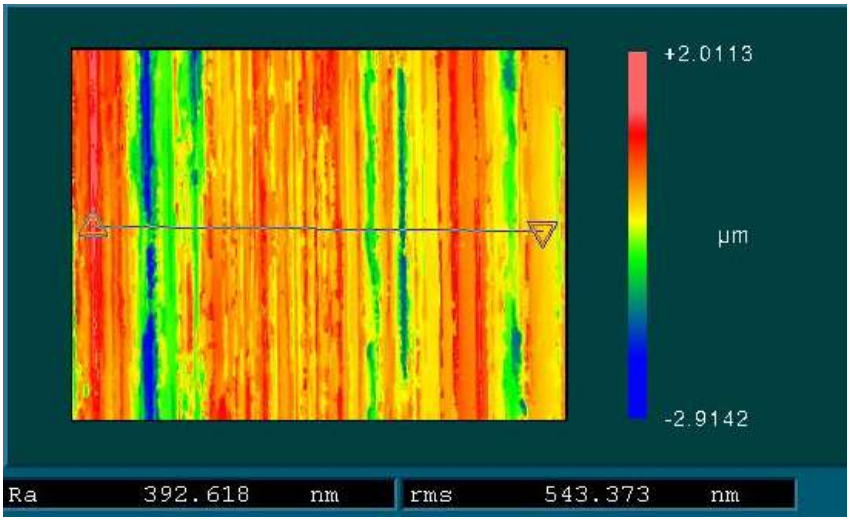

Figure 8. Surface topography of #3 brushed 304 stainless steel

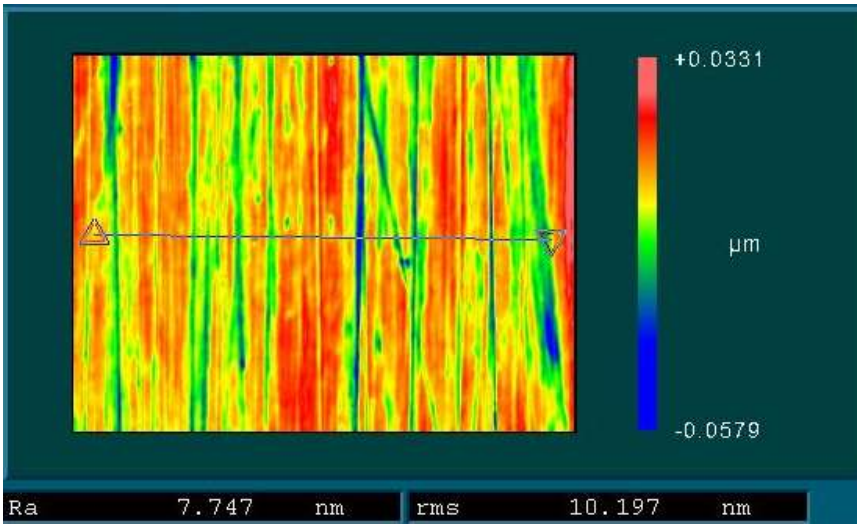

Figure 9. Surface topography of #8 "mirror polished" 304 stainless steel

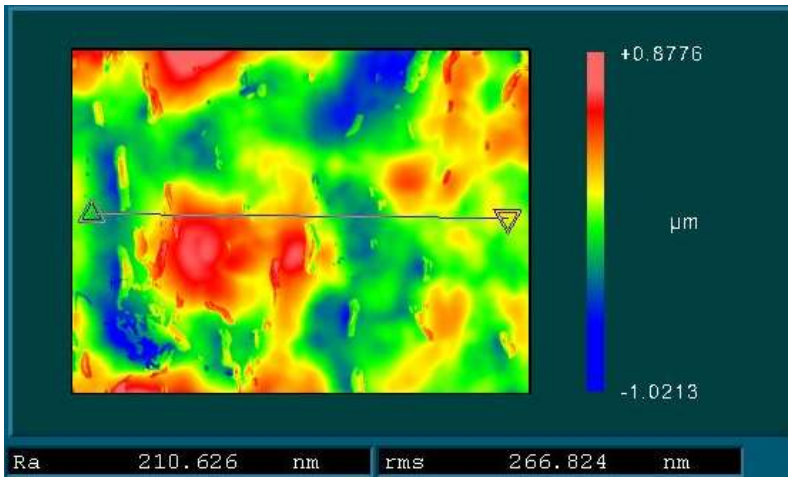

Figure 10. Surface topography of electropolished 304 stainless steel

Table I. Surface roughness measurements of experimental specimens

Material	Alumino-silicate	AS-Lapped	Boro-silicate	Soda-Lime	SS, #3	SS, #8	SS - EP
rms, mean, nm	3.8	810	4.1	2.5	510	12	310
rms, min, nm	1.6	730	1.1	0.6	400	10	260
rms, max, nm	5.3	870	13	5.8	560	16	420
R_a, mean, nm	1.8	620	1.2	1.0	380	8.8	250
R_a, min, nm	1.0	560	0.8	0.5	310	7.8	200
R_a, max, nm	2.5	650	2.3	2.7	410	11	340
PV, Mean, nm	63	9700	310	290	4700	150	2300
PV, Min, nm	26	7800	21	6.5	3400	91	1900
PV, Max, nm	84	14000	1100	1100	5500	190	2700

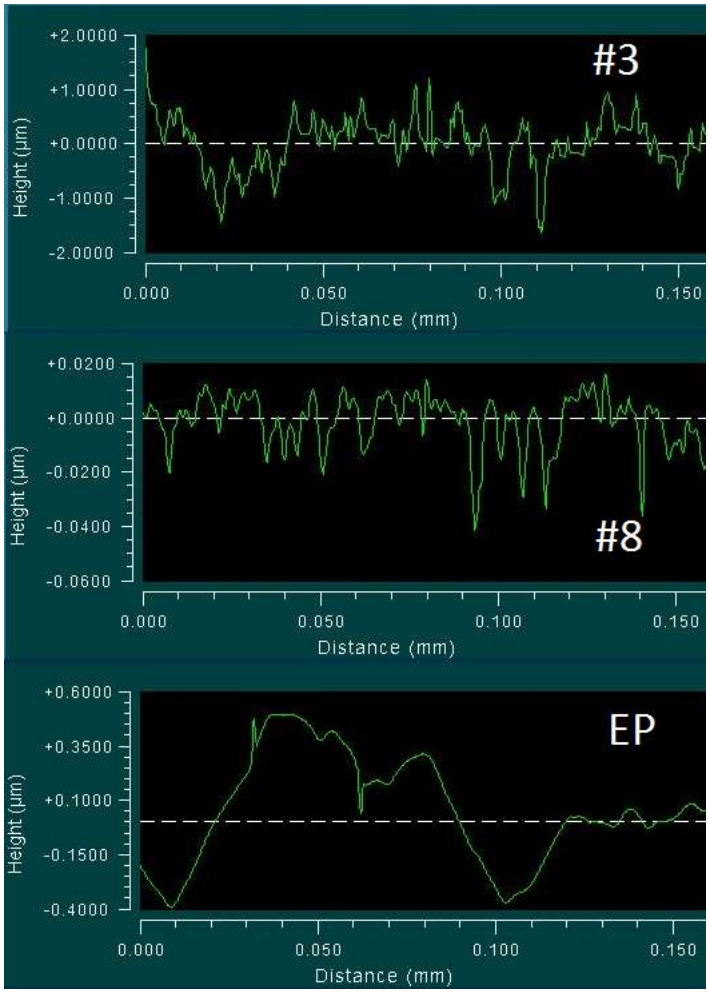

Figure 11. Cross-sectional profiles of #3, #8, and electropolished stainless steel samples

B. Contact Angle Measurements

Water contact angles were measured on the as-received glass specimens prior to any surface preparation treatments. These samples exhibited large variations in contact angle between glass types, from sample to sample, and in some instances from location to location on a single sample. The uncleaned aluminosilicate glass had contact angles from 5 to 8 degrees. The borosilicate glass had contact angles from 6 to 15 with a few outliers as high as 30 degrees. The soda-lime silicate glass had contact angles ranging from 15 to 45 degrees. All measurements were taken shortly after removing any protective film that the incoming glass was packaged in.

After heat-treating, contact angle measurements were repeated. After heat treatment, mean contact angles were less than 5 degrees for each group, and all individual samples had contact angles of less than 6 degrees.

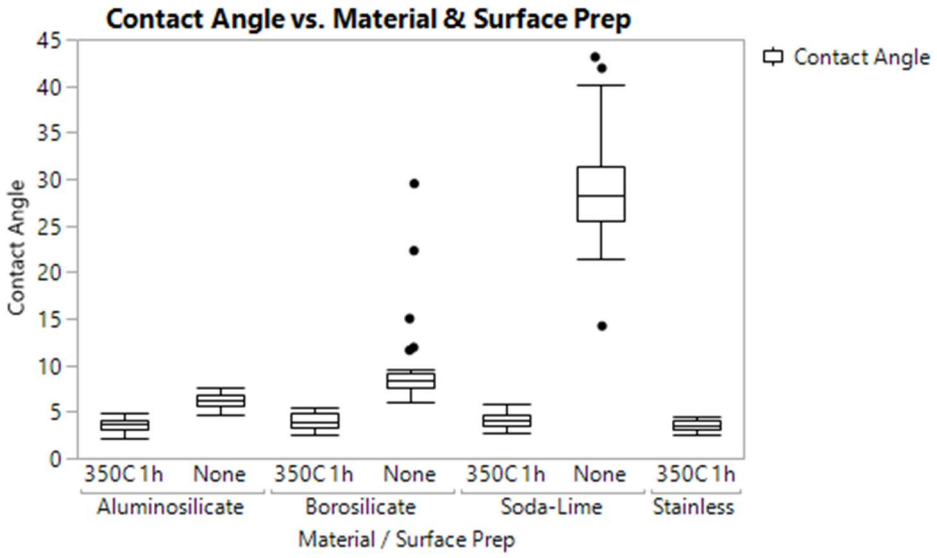

Figure 12. Measured contact angles of samples before and after thermal treatment

There was no statistically significant difference in contact angle between the borosilicate and soda-lime silicate glass after thermal treatment; The aluminosilicate glass had a statistically lower contact angle than the soda-lime glass ($p = 0.01$); the difference between the aluminosilicate glass and the borosilicate was of marginal significance ($p = 0.07$). The measured mean contact angles from are consistent other experimental work on the heat treatment of glass.[13]

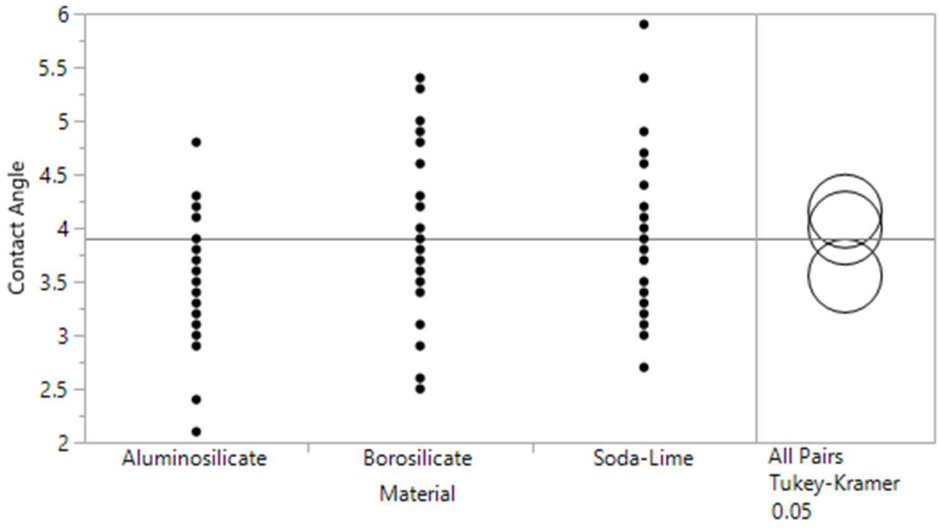

Figure 13. Comparison of contact angle measurements by glass composition

C. Friction Experimentation

Initial friction experimentation focused on glass-on-glass and glass-on-steel interactions between aluminosilicate, borosilicate, and soda-lime glasses against varying surface finishes of stainless steel at 40 +/- 5% relative humidity. Subsequent experimentation expanded the set of conditions to include the same interactions at 10 +/- 5% and 65 +/- 5% relative humidity.

For this experimental work, a full factorial design was employed. This experiment embodied 4 glass types for the top "rider" specimen, 3 humidity levels, and 4 substrate types: glass matching the top specimen, #3 stainless, #8 stainless, and electropolished stainless steel. A total of 48 experimental conditions were tested and analyzed.

1. Glass Composition Effects

For glass-on-glass friction, the aluminosilicate glass exhibited a greater coefficient of friction than the soda-lime or borosilicate glasses. This difference persists across all levels of relative humidity, and is statistically significant when the total of all glass-on-glass friction measurements are considered; when individual humidity levels are

looked at in isolation, the difference is significant at ambient humidity, but falls short of significance at dry and humid conditions.

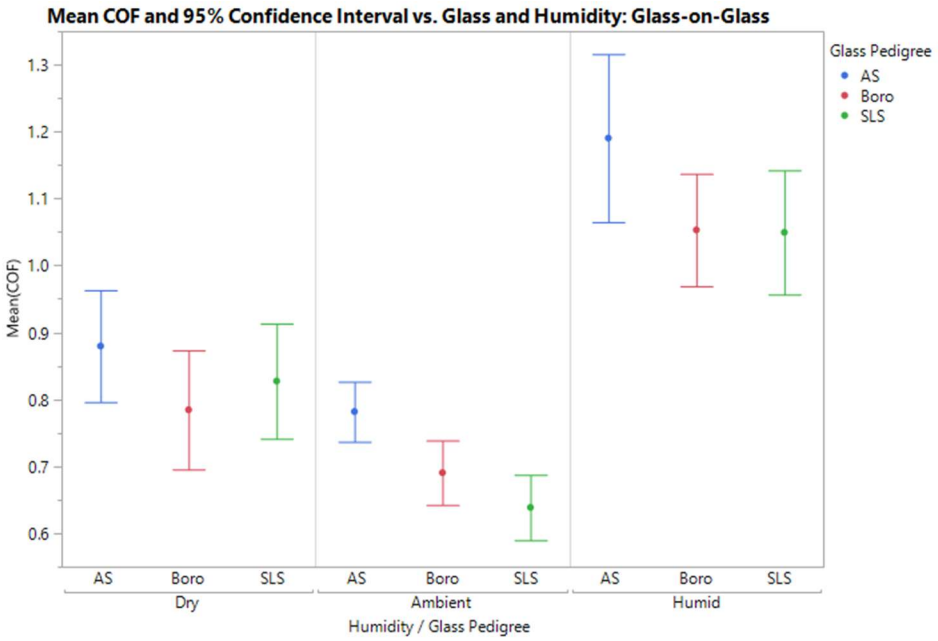

Figure 14. Mean coefficient of friction by glass composition and humidity

Table II. Statistical comparison of coefficient of friction across multiple glass compositions by humidity for glass-on-glass friction

Humidity	Glass 1	Glass 2	Difference	Std. Err	p-Value
Dry	AS	Boro	0.095	0.058	0.2396
Dry	AS	SLS	0.052	0.058	0.6439
Dry	SLS	Boro	0.043	0.058	0.7428
Ambient	AS	SLS	0.143	0.032	0.0001
Ambient	AS	Boro	0.091	0.032	0.0162
Ambient	Boro	SLS	0.052	0.032	0.2452
Humid	AS	SLS	0.141	0.069	0.1125
Humid	AS	Boro	0.137	0.069	0.1250
Humid	Boro	SLS	0.004	0.069	0.9985

For glass-on-steel friction, soda-lime glass exhibits a lower coefficient of friction than aluminosilicate or borosilicate glass. These differences are statistically significant

when the various humidity conditions are treated as an aggregate data set, as well as for a subset of specific humidity conditions.

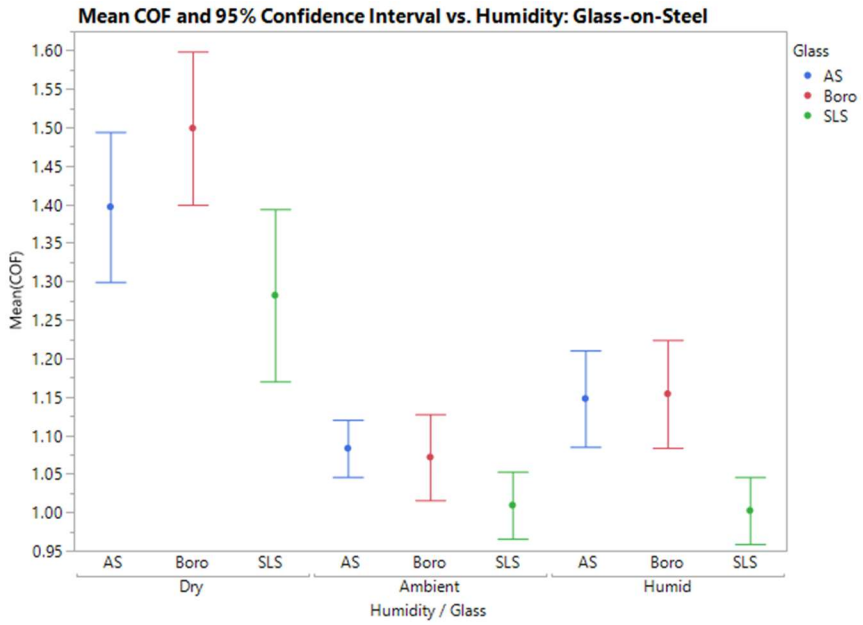

Figure 15. Mean and confidence intervals for coefficient of friction as a function of glass composition and humidity

Table III. Statistical comparison of coefficient of friction across multiple glass compositions by humidity for glass-on-steel friction

Humidity	Glass 1	Glass 2	Difference	Std. Err	p-Value
Dry	Boro	SLS	0.217	0.073	0.009
Dry	AS	SLS	0.115	0.073	0.259
Dry	Boro	AS	0.102	0.073	0.343
Ambient	AS	SLS	0.055	0.030	0.164
Ambient	Boro	SLS	0.041	0.030	0.370
Ambient	AS	Boro	0.014	0.030	0.882
Humid	Boro	SLS	0.152	0.042	0.001
Humid	AS	SLS	0.145	0.042	0.002
Humid	Boro	AS	0.006	0.042	0.988

The differing glass compositions also exhibited differing levels of within-sample friction variability. Borosilicate glass exhibited higher within-sample frictional variability, particularly under dry conditions. This behavior persisted on both glass and stainless steel substrates. Numerically this manifested as increased within-sample standard deviation. When conducting the coefficient of friction test this was visually apparent as stick-slip behavior. While this stick-slip behavior occurred for all sample types, it was much more extensive for the borosilicate glass samples than the aluminosilicate or soda-lime samples.

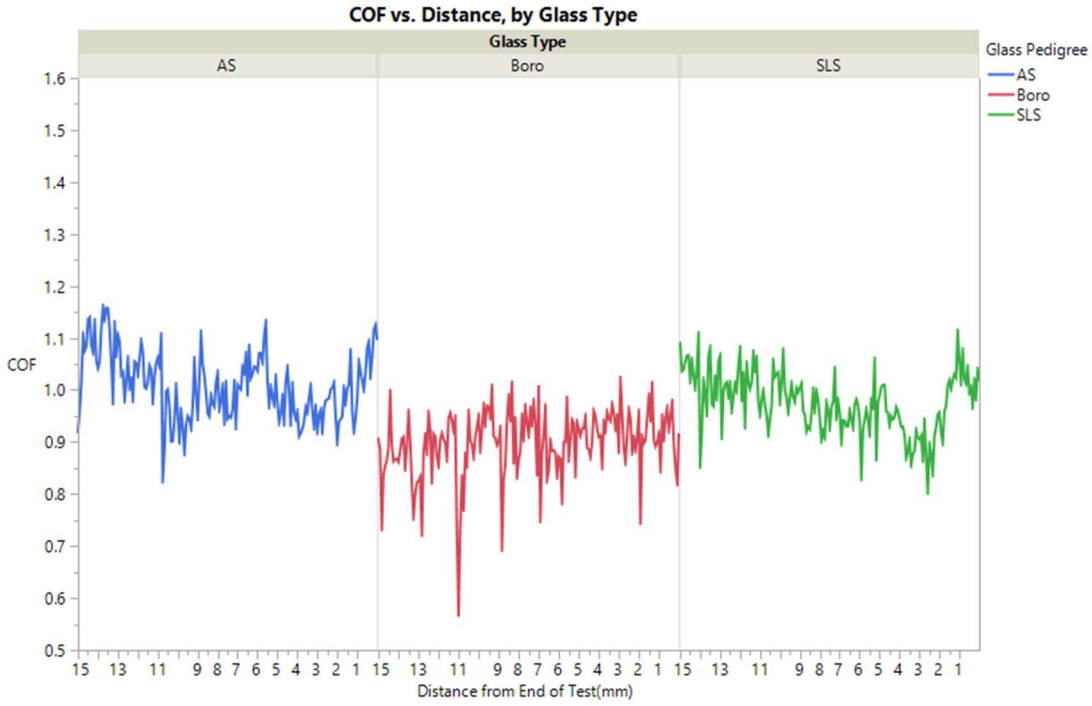

Figure 16. Individual friction plots for aluminosilicate, borosilicate, and soda-lime glass specimens illustrating typical within-sample variability

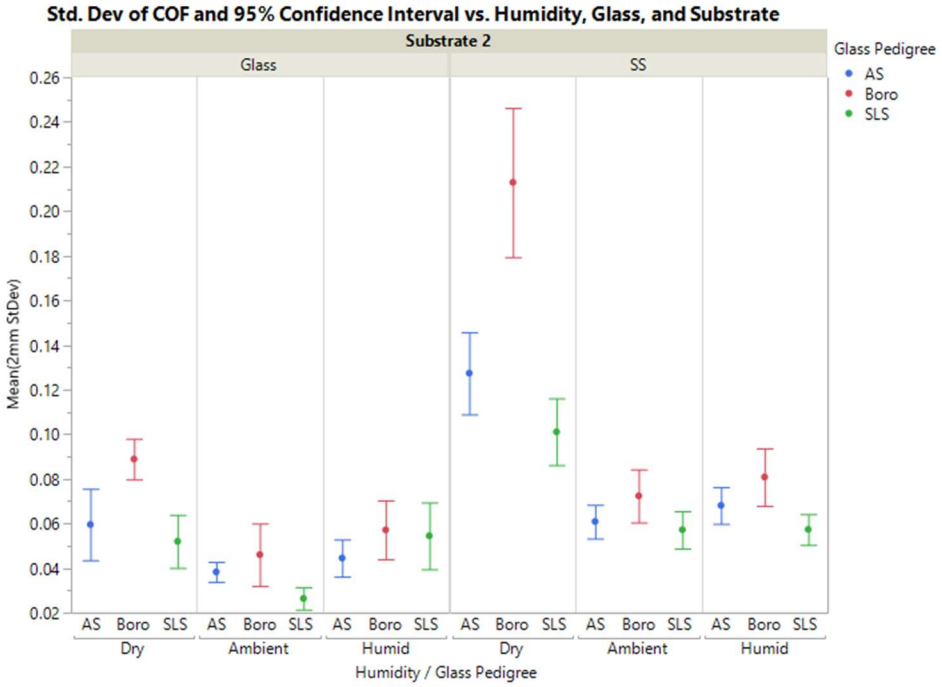

Figure 17. Means and confidence intervals for within-sample standard deviation

2. Effects of Thermal Treatment

Samples of each glass type were measured at ambient humidity before and after surface preparation. Mean coefficient of friction values typically ranged from 0.2 to 0.3 before thermal treatment and 0.65 to 0.8 after thermal treatment. The latter values are consistent with literature values for glass-on-glass friction for clean specimens. The glass-on-glass coefficients of friction also track inversely to the measured contact angles for each glass type both before and after thermal treatments.

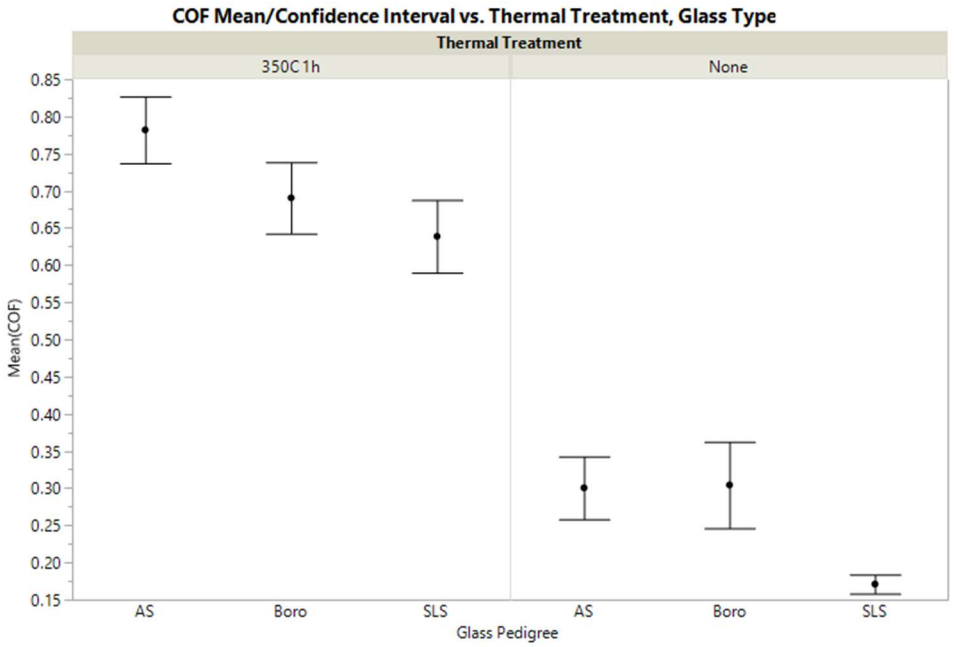

Figure 18. Means and confidence intervals for coefficient of friction as a function of glass composition and surface preparation

Data was analyzed as a function of test order to examine whether there were any time-based effects that could be attributed to recovery of surface water or accumulation of organics on specimen surfaces. There was no evidence of any time-based effects when examining mean glass-on-glass friction versus run order across multiple sample sets. For glass-on-steel testing, the first sample tested in each set has a higher mean friction than the later samples tested, and the difference between the second sample tested and the remainder of the data set is of marginal significance.

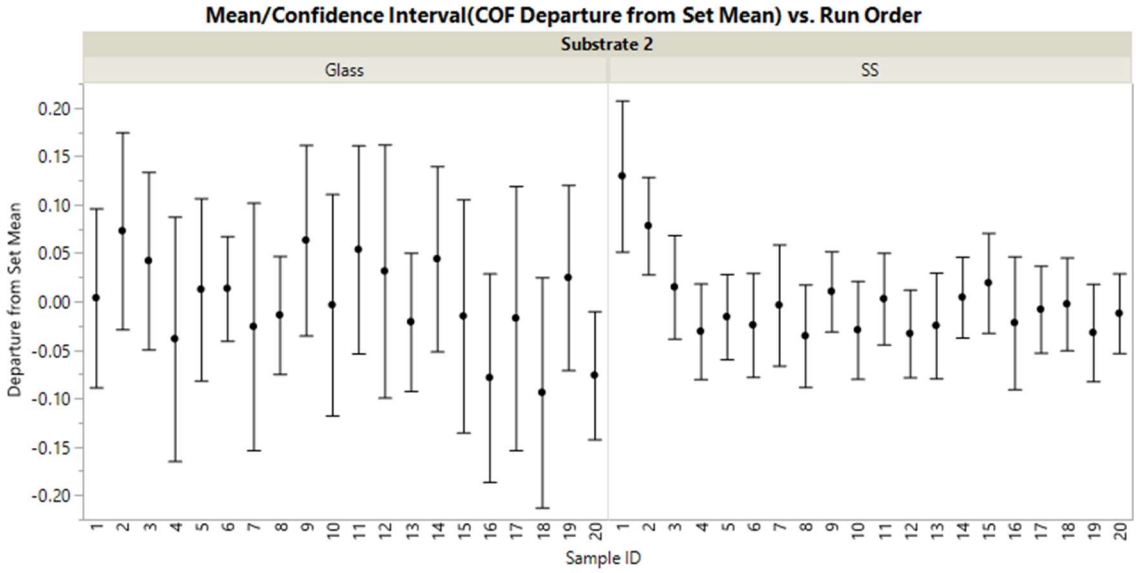

Figure 19. Mean and confidence intervals for coefficient of friction as a function of run order for glass-on-glass and glass-on-steel friction testing

3. Impact of Roughness and Humidity on Friction

The potential for interaction between surface roughness and humidity is well-documented in literature. Many of these interactions are evident in the experimental conditions. A comparison of lapped aluminosilicate glass with smooth, as-formed samples illustrates this interaction clearly.

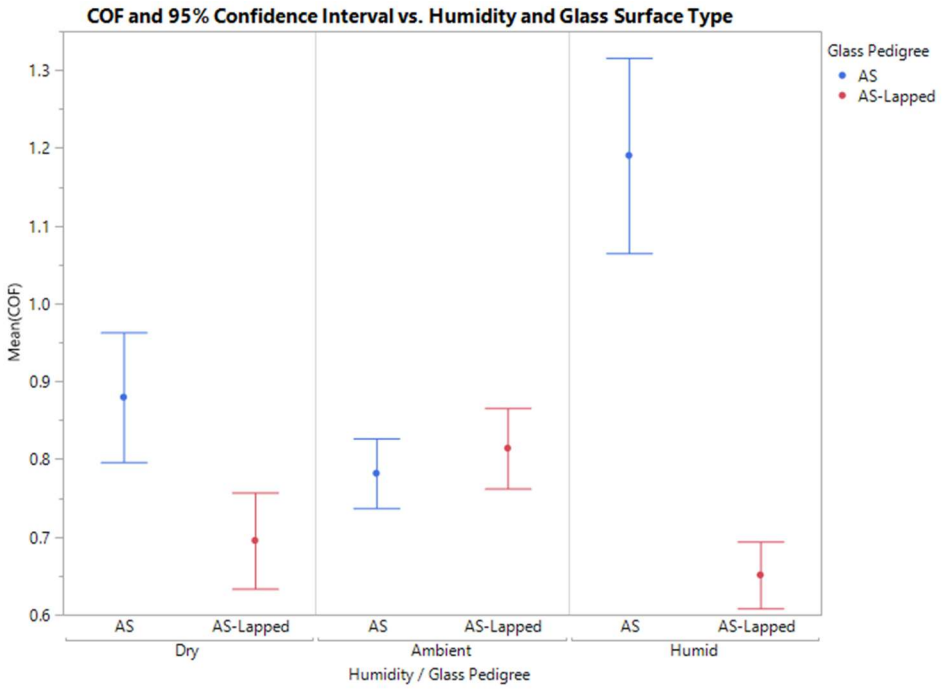

Figure 20. Comparison of coefficient of friction for lapped versus as-received aluminosilicate glass as a function of humidity

While the two surface preparations exhibit similar coefficients of friction at ambient humidity, the smooth surface exhibits an increase in friction at both low and high relative humidity, while the lapped sample exhibits a decrease. For glass-on-steel interactions, this divergence was similar, but more complex.

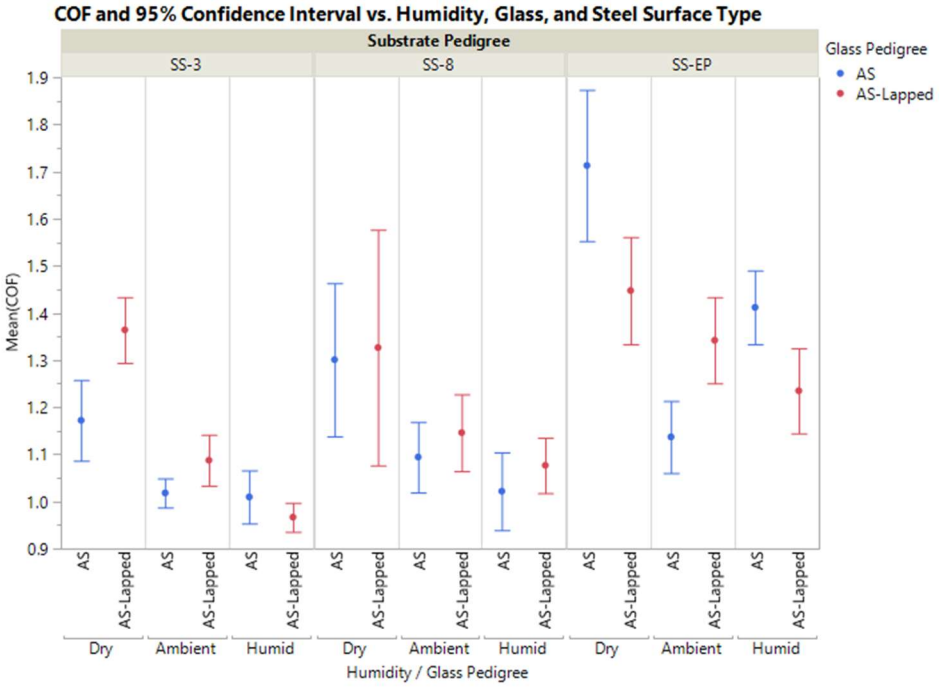

Figure 21. Coefficient of friction for aluminosilicate glass on steel as a function of glass roughness, humidity, and steel surface finish

There are two distinct sets of behavior for glass on steel friction: the #3 and #8 stainless steel substrates as well as the lapped aluminosilicate on electropolished steel exhibit decreasing friction with increasing relative humidity. Conversely, smooth aluminosilicate glass on electropolished stainless steel behaves similarly to glass-on-glass friction, with a local minimum at moderate humidity, and increased friction at both low and high humidity levels. The increase in friction under dry conditions was much greater for glass on steel than it was for glass on glass.

This data can be further simplified into two types of interactions: “smooth on smooth” interactions, defined as a system where both surfaces are either electropolished stainless steel or as-formed or polished glass, and “Rough”, where at least one surface was subject to a mechanical process yielding a rougher surface. Analyzing the data through this categorization makes trends much clearer:

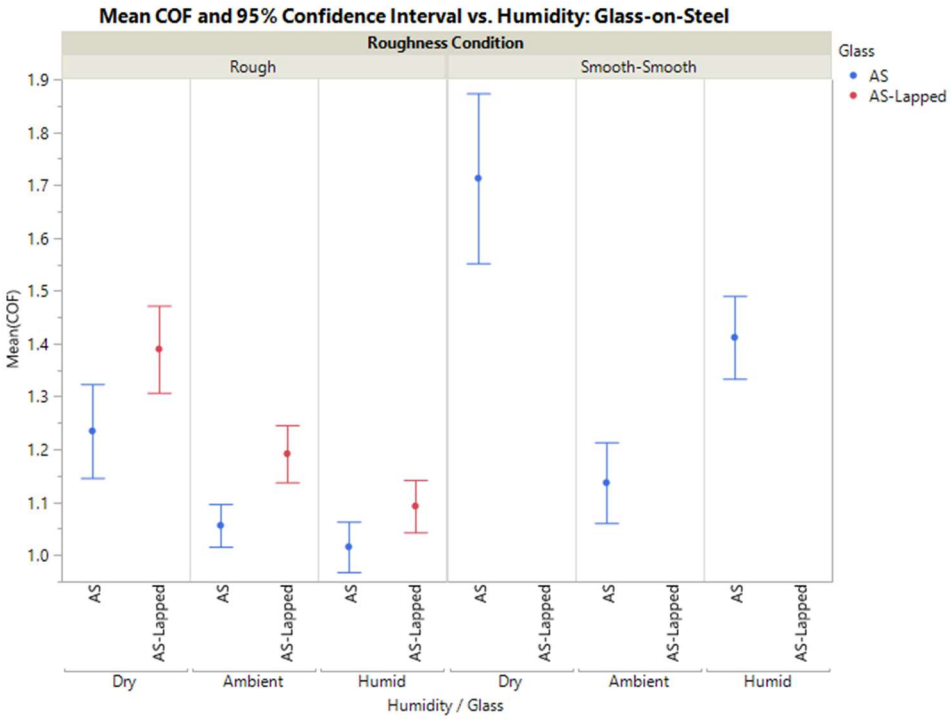

Figure 22. Comparison of friction between smooth and rough interactions for aluminosilicate glass-on-steel friction

Rough interactions exhibit a distinctly different trend than smooth-on-smooth interactions in all cases. Furthermore, rough interactions involving a lapped aluminosilicate sample exhibit a higher coefficient of friction than rough interactions involving smooth aluminosilicate glass on roughened steel. A similar trend is evident for the rough samples when looking at the impact of steel finish: Smooth/electropolished steel on a rough/lapped glass substrate exhibits as higher coefficient of friction than rough/mechanically-finished steel on a smooth glass substrate.

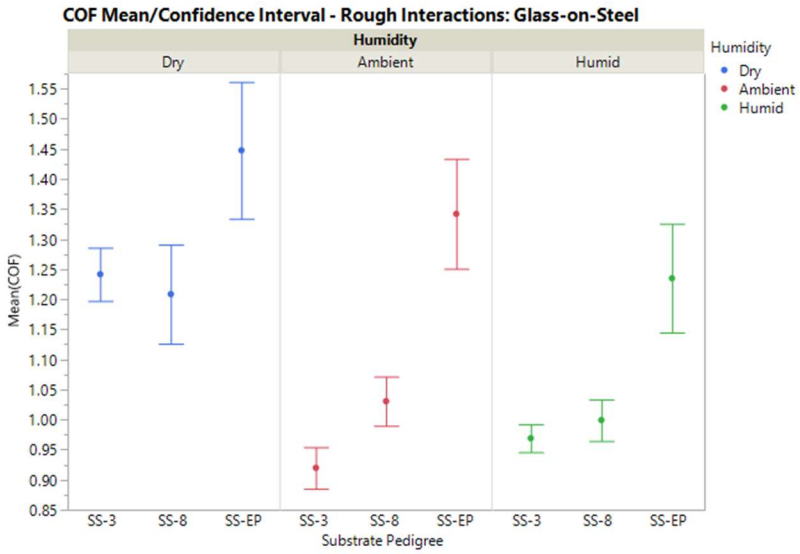

Figure 23. Mean and confidence intervals of coefficient of friction for rough glass-on-steel interactions

Furthermore, there are distinctly different trends not only in mean friction, but in variability and local frictional behavior as a function of both roughness and relative humidity. Particularly for smooth-on-smooth interactions, there is a clear decrease in within-sample variation with increasing humidity, as quantified by the coefficient of variation metric. When observing testing of individual samples and examining the test data, this manifests as a progressive decrease in observable stick-slip friction events with increasing relative humidity.

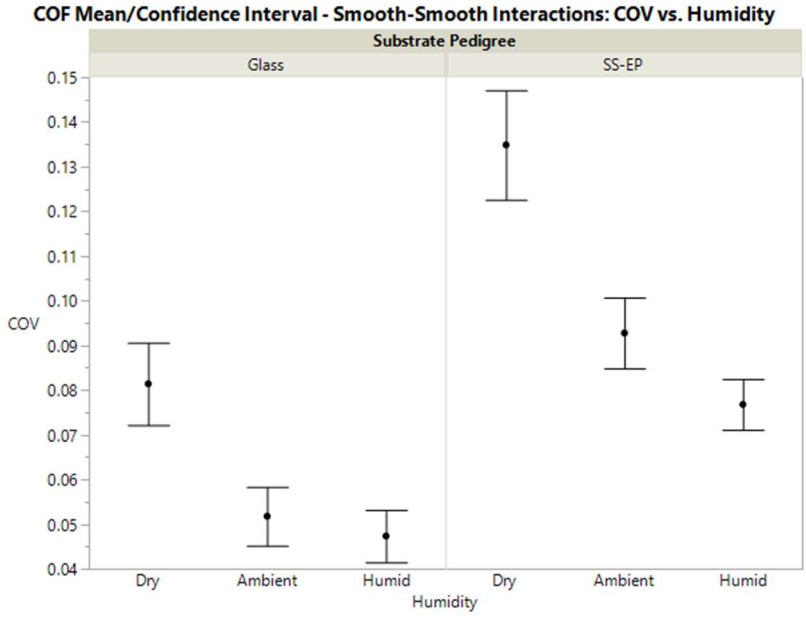

Figure 24. Coefficient of variation versus humidity for smooth-on-smooth interactions

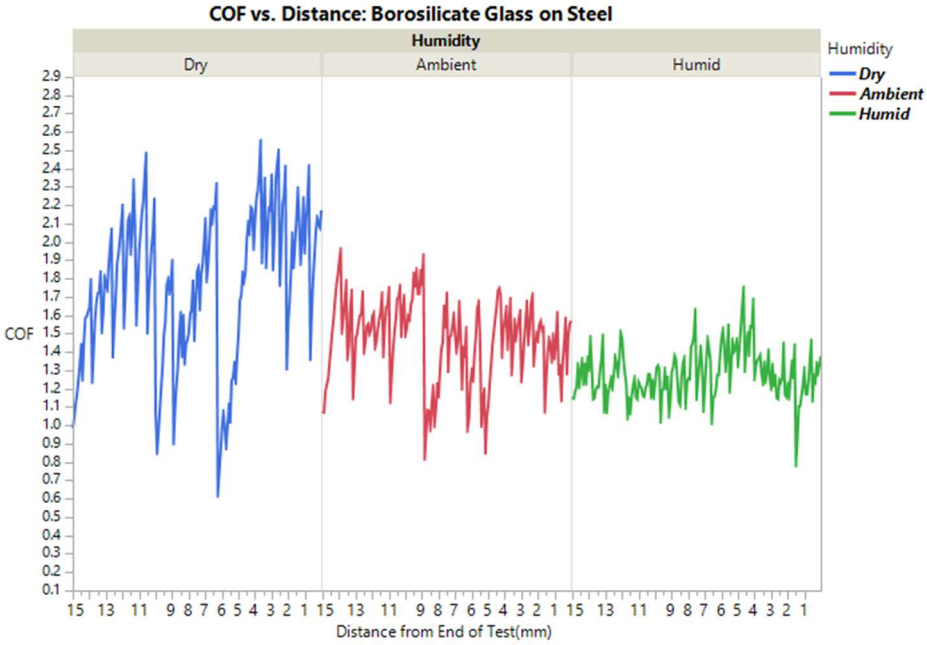

Figure 25. Individual coefficient of friction plots as a function of humidity for borosilicate glass

Analysis of the impact of surface roughness reveals a similar trend with respect to stick-slip events: the rougher samples are much less prone to significant stick-slip behavior and exhibit significantly lower within-sample variability. This is evident in the friction plots for individual samples as well as the COV metric, and is particularly prominent under dry conditions.

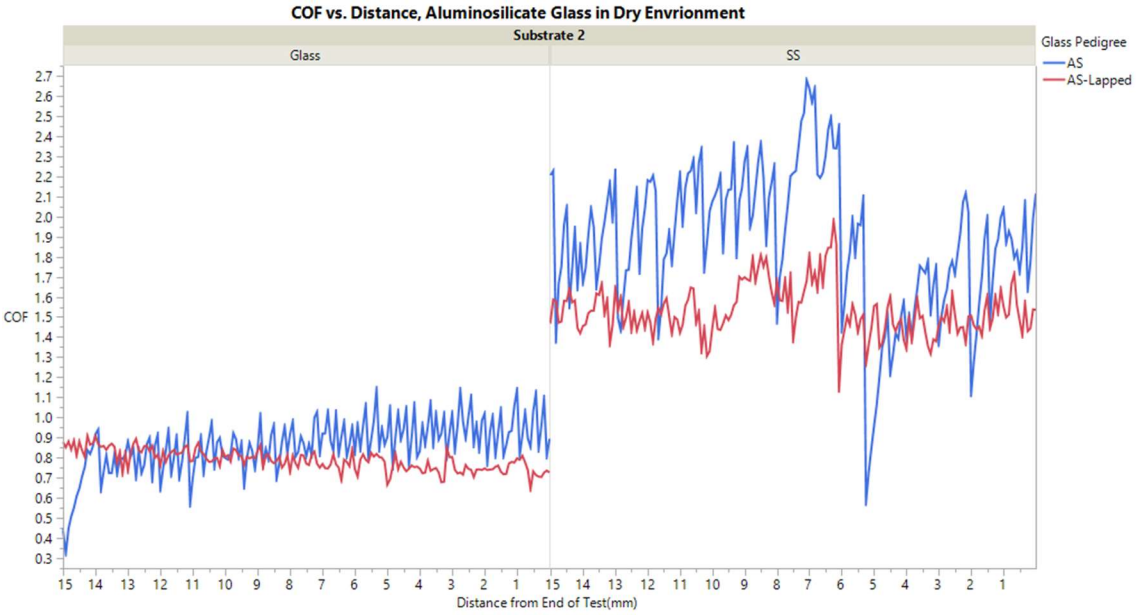

Figure 26. Individual coefficient of friction plots for lapped and as-received aluminosilicate glass on glass and electropolished steel under dry conditions

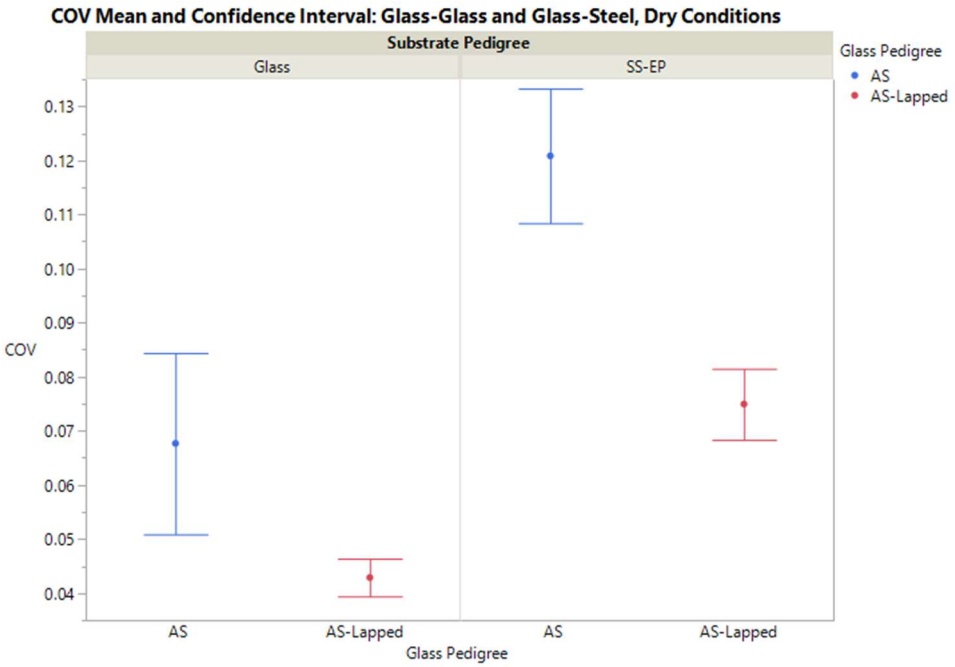

Figure 27. Coefficients of variation of lapped and as-received aluminosilicate samples against glass and electropolished steel under dry conditions

4. Wear and its Effects

To assess potential impacts of wear on measured friction over the length of a test, friction as a function of position was aggregated across multiple tests. This data was evaluated to assess whether friction rose, fell, or remained constant over time for a range of conditions. For glass-on-glass friction, lapped samples exhibited stable or decreasing friction over the length of friction tests, while smooth surfaces exhibited a gradual increase in friction. These effects were most pronounced at the driest and most humid conditions tested. For glass-on-steel friction, the relationship between coefficient of friction and test duration was even more consistent. Stainless steel substrates consistently exhibited an increase in mean friction over the duration of the test. This behavior was particularly pronounced at low humidity.

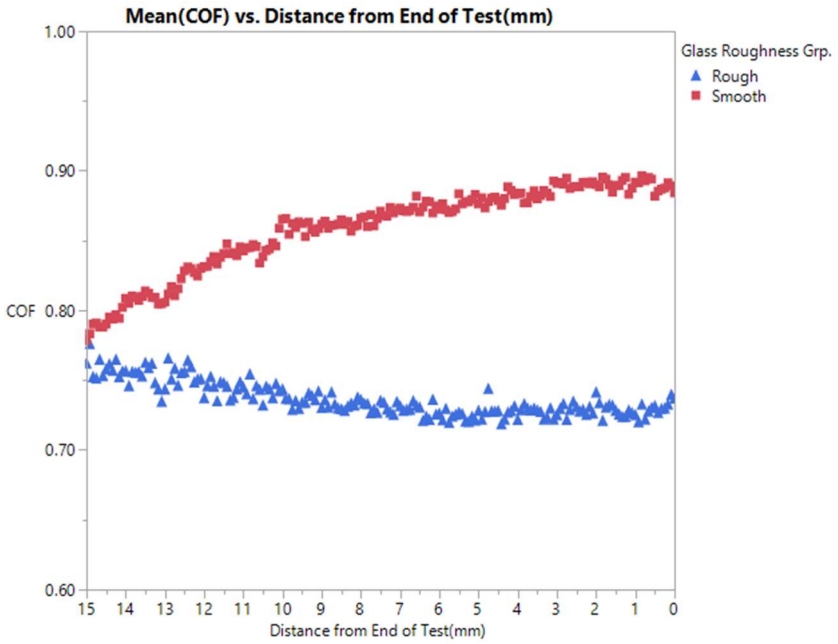

Figure 28. Mean coefficient of friction versus distance for glass-on-glass friction comparing lapped and smooth glass samples

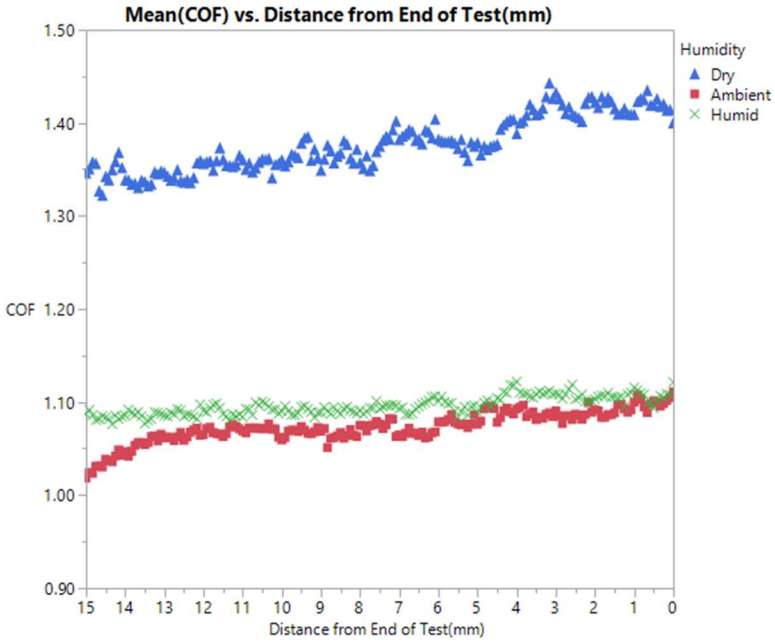

Figure 29. Mean coefficient of friction versus distance for glass-on-steel friction as a function of relative humidity

Glass and stainless steel specimens were examined via optical microscopy and images of the surfaces of select samples were captured after friction testing to assess the extent and nature of wear that occurred during friction testing. Parts were selected for assessment from observation of visible wear tracks. These samples were measured via profilometry and optical microscopy to assess the impact of the friction events on both the glass specimens and the steel substrates.

At high humidity levels, wear on glass and steel specimens was difficult to observe. Wear was visually most apparent at low-humidity conditions and on samples that had locally high friction measurements during testing. Evidence of wear was also difficult to observe on roughened samples due to the surface texture obscuring any visible wear, as well as reduced wear severity associated with lower maximum coefficients of friction.

Cross-sectional profiles and topography of wear tracks were measured. The most severe wear tracks corresponded to deformations of 50 microns or more to the stainless steel surface.

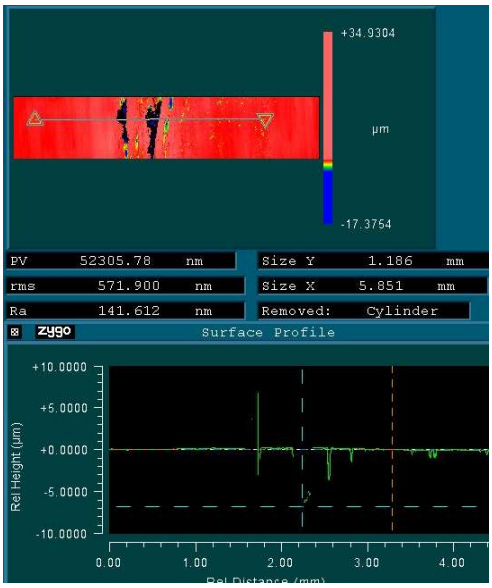

Figure 30. Topography of wear track for #8 stainless steel samples after friction with aluminosilicate glass under dry conditions

Compared with roughness measurements of approximately 10 nm on clean #8 stainless steel substrates, the topography of the wear tracks was several orders of magnitude greater. This suggests that there was significant mechanical alteration of the stainless steel surfaces under these conditions.

Optical microscopy of stainless steel surfaces revealed several defining features of frictional wear. Typical wear tracks were on the order of 500 to 1000 microns wide. Within these wear tracks there was evidence of the materials tracking across each other, but there was also evidence of alteration of the stainless steel surface itself, as evidenced by the discoloration. There were also numerous pitted areas with soft edges, with apparent removal of material from the stainless steel surface. Additionally, there is evidence of particles in the path of the wear track, suggesting some material removed from either the glass or the stainless steel surface ended up as debris in the wear track.

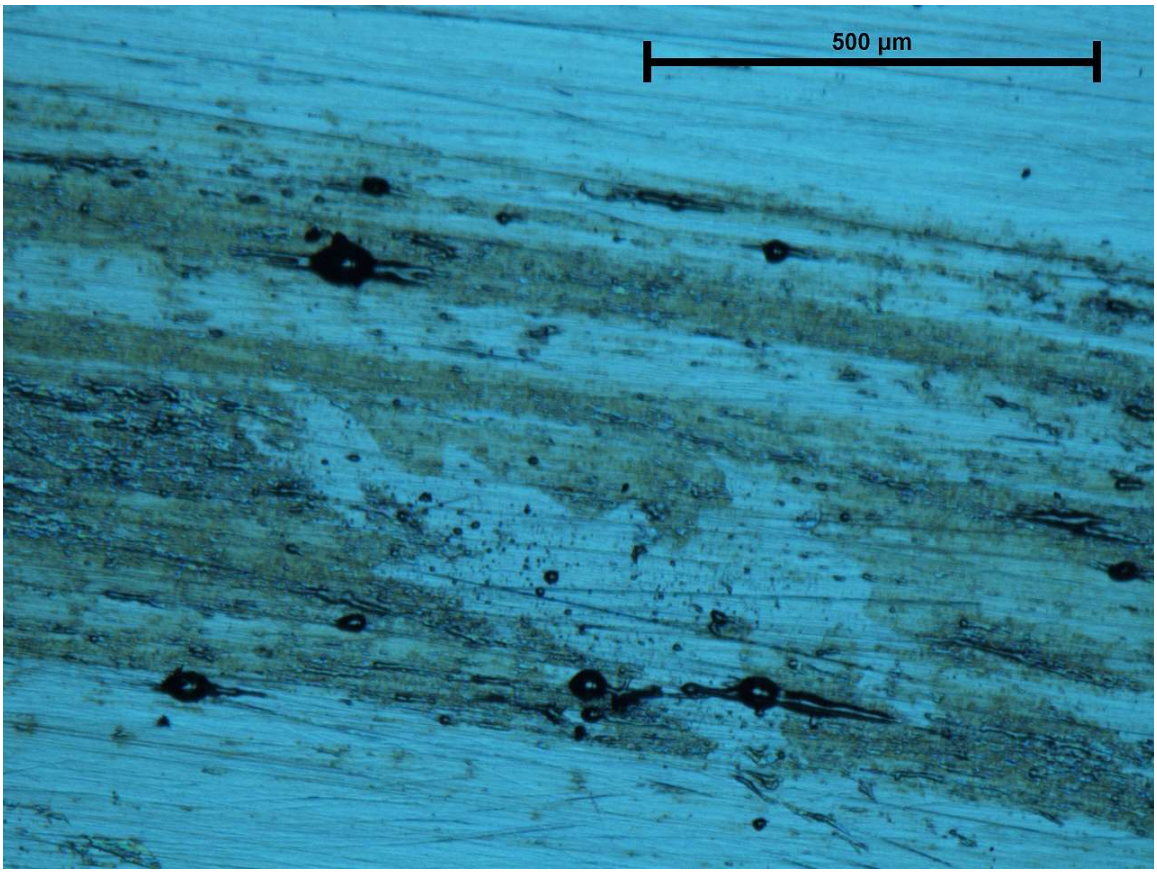

Figure 31. Microscope image of stainless steel after dry frictional events

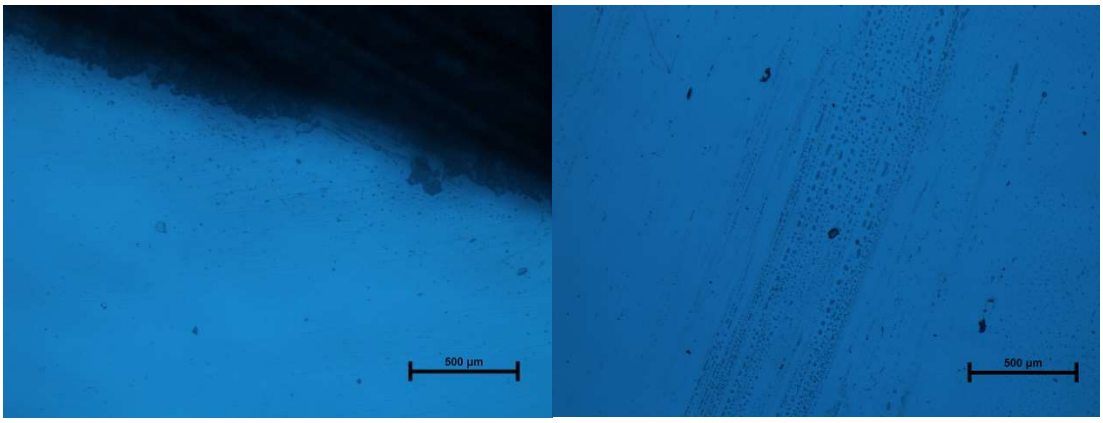

Figure 32. Microscope images of edge damage and material transfer on borosilicate glass

The glass samples exhibited evidence of edge damage from the friction testing, as well as scattered particles on the glass surface resulting from this damage. Additionally, there were localized tracks several hundred microns in width where there was apparent material transfer from the stainless steel substrate to the glass surface. Further examination revealed that this material was loosely adhered and could be removed through light mechanical action.

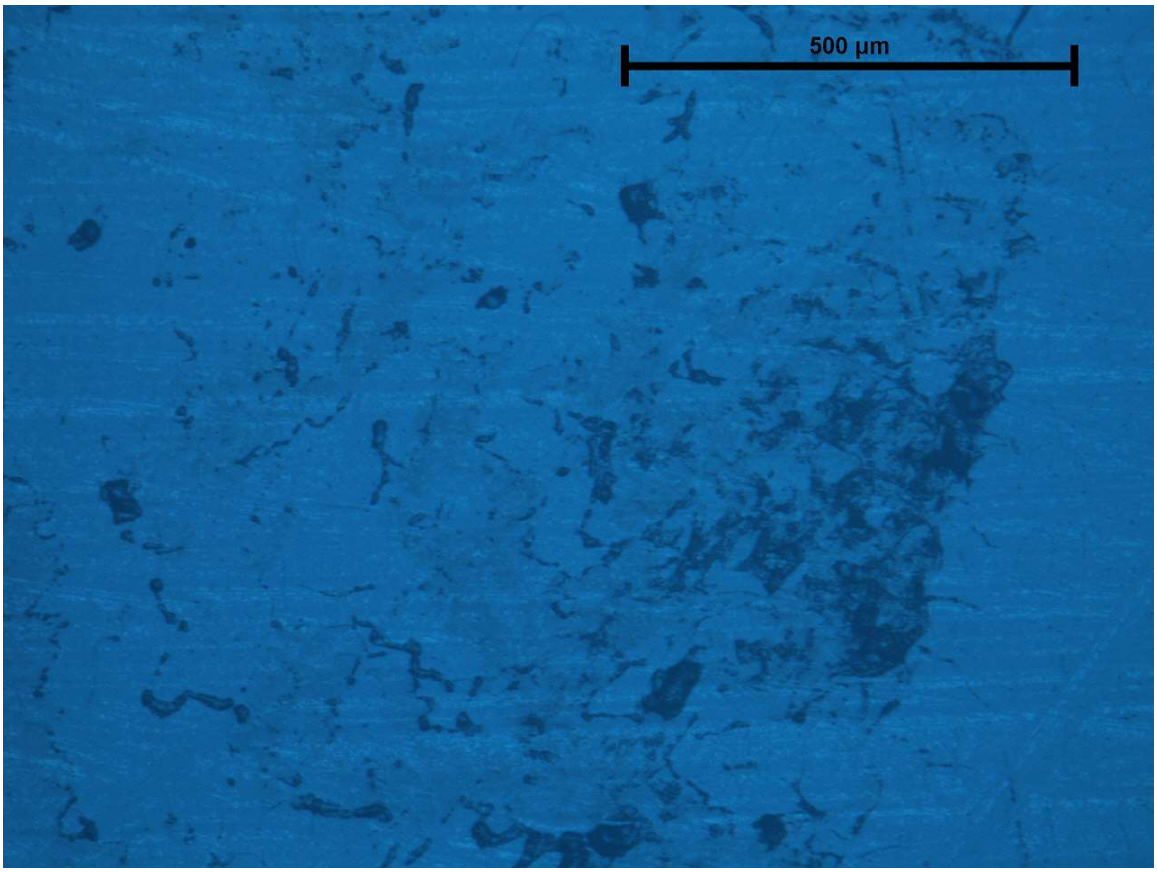

Figure 33. Microscope image of metal transferred to aluminosilicate glass surface

The appearance aluminosilicate and soda-lime glass samples were after friction testing was similar that of borosilicate glass. The material in the wear tracks on the glass surface did not have the appearance of fractured glass particles; it had an appearance under ambient lighting that is consistent with oxidized stainless steel. This material was not well-adhered to the glass surface and was removable with light mechanical action. There was no evidence of surface cracking or other glass damage in this area of the glass.

In all cases the wear tracks were not uniform over either the stainless steel or glass specimens; in most cases the track lengths comprised a significant fraction of the test length, but the width of the wear area was a few millimeters or less. This implies that contact frequently occurred over a small fraction of the overall sample area, and that sample flatness was a major determinant of the contact area between samples.

V. DISCUSSION

A. Thermal Treatment

The standard thermal treatment of 350C for 1 hour was effective at providing a consistent, uniform glass/metal surface for the purposes of experimentation. This is consistent with the work of previous authors, including Butz[13] and Jenkins.[14] The data strongly supports that these treatments were effective at removing organic residue from the surface of the glass specimens, as the contact angles ranged from 2 to 6 degrees for every sample measured, and the measured ambient-humidity coefficients of friction ranging from 0.64 to 0.81 are consistent with literature values for clean glass at typical ambient humidity.

Measurement results for coefficient of friction as a function of time and test order after thermal treatment did not exhibit any time-related trends for glass-on-glass friction testing. This supports the conclusion that the equilibration time between thermal treatment and testing of these samples was sufficient for the surfaces of the glass specimens to reach equilibrium or near-equilibrium with the environment with respect to surface hydroxylation. This is consistent with the work of D'Souza and Pantano,[16] who found rapid re-hydroxylation of glass surfaces after thermal treatment for short durations at temperatures 350C or below. The absence of a significant downward trend with time also suggests that the duration the friction testing was sufficiently short that the accumulation of surface organics did not have a significant impact on the test results.

Conversely, the experimental data suggests that surface conditions may not have reached a true equilibrium prior to the first samples tested for glass-metal friction testing. The first two samples tested exhibited a higher mean coefficient of friction than the remainder of the samples for any given sample set when the experimental data for all conditions was examined in aggregate. The most plausible explanation for this phenomenon is the thermal mass of the stainless steel substrates. The stainless steel substrates are significantly more massive than the glass specimens, and they took noticeably longer to cool due to their increased heat capacity. While the glass specimens were not perceptibly different from room temperature at the initiation of testing, the steel

substrates were still perceptibly warm 10 to 15 minutes after thermal treatment. This elevated temperature creates a different local environment at the glass/steel interface, resulting in a relative humidity below that of the surrounding environment, thereby limiting the resorption of surface moisture after thermal treatment. Considering that all glass-steel combinations exhibited significantly increased friction at low humidity, it is probable that these samples had lower levels of adsorbed water on the glass surface prior to cooling completely and thus exhibited elevated coefficients of friction like those that would be associated with lower humidity.

B. Glass Composition

The varying glass compositions tested in this work exhibited differences in measured coefficients of friction under some circumstances, although the influence of glass composition was a much weaker effect than the interaction between surface roughness and humidity.

Aluminosilicate glass exhibited a higher mean coefficient of friction than either borosilicate glass or soda-lime glass for glass-on-glass friction, particularly at moderate humidity levels. When combined with the aluminosilicate glass specimens having the lowest measured contact angle of the glass compositions, this is consistent with the aluminosilicate glass having the highest surface energy of the glass compositions, and hence being the most likely to exhibit a high level of adhesion.

Additionally, the frictional behavior of the borosilicate glass samples was distinctly different from the other specimens. Prominent stick-slip events occurred with much greater frequency on the borosilicate glass samples when compared with either aluminosilicate or soda-lime silicate glasses, particularly in dry environments. One potential explanation for this behavior is the greater hardness of borosilicate glass when compared with either soda-lime or aluminosilicate glass that has not been ion exchanged, as reported by He, Qian, Pantano, and Kim.[21] In an environment where material fracture is constrained by limited water availability, the mechanical properties of the base material become increasingly significant in determining its frictional behavior. This behavior is also consistent with a second observation of the same team that borosilicate glass was

less prone to wear than either soda-lime or aluminosilicate glass.[21] If the glass surface is more durable, it may take more force to break bonds at that surface, resulting in a higher static coefficient of friction and a greater tendency toward stick-slip events.

Soda-lime glass exhibited a lower coefficient of friction than the other glass compositions against stainless steel. The lower hardness and greater susceptibility of soda-lime glass to aqueous attack via stress corrosion mechanisms are both consistent with the lower mean coefficient of friction of soda-lime glass over a broad range of humidity.

C. Roughness, Humidity, and Wear Effects

There were several distinct, non-linear trends when looking at the interaction of humidity and surface roughness. For smooth surfaces, friction at both dry and humid conditions was greater than at ambient humidity. The increase in dry friction was more substantial for glass-steel friction, while the increase in humid friction was more substantial for glass-glass friction. Additionally, samples with rougher surfaces exhibited significantly lower within-sample and sample-to-sample variation than smooth-on-smooth interactions for most conditions. This is the product of several important interactions, all of which relate to the diverse roles that water plays in frictional interactions involving glass.

First, water can act as a chemical agent, aiding in the hydrolysis of Si-O bonds near the glass surface. Mechanically-assisted hydrolysis of bonds in glass and ceramic materials occurs via a mechanism known as stress corrosion, where oxide bonds stretched by mechanical forces are chemically attacked and hydrolyzed by water. The governing equation for this mechanism was first proposed by Charles and Hillig, and takes the form:

$$v = v_0 exp\left(\frac{-E^+ + V^+\sigma_{tip} - \gamma V_M/\rho}{RT}\right) \qquad (3)$$

In this equation, E^+ is activation energy for an unstressed bond on a flat surface, $V^+\sigma_{tip}$ is the modification of this term by stress σ over an activation volume V^+, and $\gamma V_M/\rho$ reflects the effect of surface curvature, where γ is the surface energy of the material, V_M is its molar volume, and ρ is the radius of curvature of the feature.[37] Embedded in E^+ is the influence of humidity: the reaction rate is effectively proportional

to *exp* (P_{H2O}), and the partial pressure of water is proportional to humidity.[38] Thus, maintaining an equivalent rate of bond breakage at reduced humidity requires greater surface stress and hence, a greater coefficient of friction.

The increased in measured friction at low humidity may also be driven by the unique properties of metallic substrates. Near asperity tips on the stainless steel sample, the shear stress may exceed the yield stress of the metal, and instead of experiencing brittle fracture or stress corrosion like glass or ceramics, the steel specimen may undergo ductile transformation. This results in broader, flatter asperities with increased contact area, and a further increase in coefficient of friction.

Conversely, roughening of the glass surface serves to reliably limit the maximum potential contact area, as it will not undergo ductile transformation like stainless steel. This is clearly supported by the lower friction of the lapped aluminosilicate samples relative to the other glass samples for both glass-on-glass and glass on electropolished steel interactions at low relative humidity. Additionally, the lapped aluminosilicate samples exhibit substantially lower within-sample variability under dry conditions. This suggests that the impact of ductile asperity broadening on peak friction and the potential for large adhesion events is muted by the surface roughness of the lapped samples. Roughening of a brittle surface creates a persistent limit on contact area, and hence caps the potential for substantial stick-slip events; this theoretical prediction aligns with the observation that these events were comparatively rare and minor for roughened samples during the testing process.

Additional supporting evidence for the role of the ductile transformation mechanism in the frictional behavior of glass-on-metal interactions is provided by analysis of mean friction versus test distance: Mean friction increased over the length of the test for glass-on-metal friction under all conditions, but this phenomenon was most prominent under the low-humidity conditions. This is consistent with the increased durability glass surfaces possess and the higher mean friction measured under these conditions resulting in greater shear forces on the steel substrate. These forces can exceed the yield stress of the metal at asperity tips, flattening asperity peaks. This broadening results in a larger effective contact are and increased friction between samples. At elevated humidity this effect is less prominent, as water availability results in an

increased rate of bond breakage at the glass surface. Surface tension effects associated with increased contact area of water films also serve to spread the frictional force more evenly over a larger area. Combined, these effects reduce the local shear forces on asperities and the resulting the potential for deformation.

This work and other literature provide evidence that the nature of frictional interactions changes with increasing humidity. Both glass and stainless steel surfaces adsorb increasing amounts of water to their surfaces as relative humidity increases, ranging anywhere from a monolayer to tens of nanometers depending on environmental conditions and surface chemistry. The extent to which this layer impacts frictional behavior is dependent upon its topography and the fraction of the liquid layer that contacts another surface.

The results for this experimental work are completely consistent with Tabor's observations that while humid environments increase adhesion for glass interactions, this effect is substantially muted by surface roughening.[20] Conditions where at least one of the samples had a significant degree of roughness exhibited minimal change in measured friction between 40% and 65% relative humidity, while between two smooth samples exhibited substantial friction increases over the same range of humidity. This is because the total surface separation created by asperities on rougher surfaces results in a separation greater than the sum of the adsorbed water layers on both samples. Under these conditions, the contribution of surface tension to adhesion and friction is minimal. Conversely, for interactions where surface roughness is similar to or less than the thickness of the adsorbed water films, the water layer substantially increases effective surface contact and hence adhesion and friction.

The behavior of electropolished stainless steel surfaces as "smooth" surfaces while mechanically-finished surfaces behave as "rough" surfaces was also particularly striking. While conventional R_a and rms roughness metrics define the electropolished surface as substantially rougher than the mechanically-polished #8 surface and of similar roughness to the #3 surface, profilometry reveals a surface that is much smoother/less-sloped over short distance scales. The reduced curvature and shallower slopes near asperity peaks on the electropolished surface would allow for a greater effective contact area. This curvature of asperity tips is not captured by conventional surface roughness

metrics, but the increase in effective contact area it creates manifests as an increase in coefficient of friction across all glass preparations and humidity conditions.

Additionally, this larger asperity radius has the potential to increase the adhesive contribution of adsorbed surface water films, thereby explaining why the electropolished stainless steel samples exhibit increased friction at high humidity while the mechanically-polished samples do not. Tabor put forth the following theoretical calculation of the adhesion due to a liquid film for a spherical bead:

$$Z = 4\pi R\gamma \cos\alpha \qquad (4)$$

Where Z is adhesive force, R is the surface radius, γ is surface tension, and α is the angle between two surfaces.[20] From this equation, it is evident that an electropolishing process that rounds off rough/sharp asperities will increase both R and decrease α, thereby increasing the predicted adhesion due to liquid films. Tabor also notes the importance of the relative heights of surface asperities versus adsorbed films, although in doing so he does not directly address the hypothetical case represented by an electropolishing process, whereby it is possible to have relatively large, but round/smooth asperities, although the equation put forth clearly predicts this behavior.

VI. SUMMARY AND CONCLUSIONS

From analysis of dynamic coefficients of friction of aluminosilicate, borosilicate, and soda-lime glasses against glass and stainless steel substrates of varying surface roughness, the following can be concluded:

1. Coefficient of friction measurements taken in dry conditions yielded higher average coefficients of friction than those performed in ambient humidity. This effect was most pronounced for smooth-on-smooth interactions, and can likely be attributed to the reduced availability of water to participate in chemomechanical bond breakage at the glass surface as well as ductile broadening of asperities increasing effective contact area.
2. The effects of higher humidity were substantially interactive with surface roughness. Smooth-on-smooth tests consistently exhibited an increase in coefficient of friction with increasing humidity, while smooth-on-rough or rough-on-rough combinations exhibited neutral or decreasing friction with increasing humidity. This effect can be attributed to the relative thickness of adsorbed water layers on glass and stainless steel surfaces in comparison with the roughness of those surfaces impacting the effective contact area of water films between those two surfaces, and the resulting surface tension affects creating adhesive force.
3. The principal mechanism of wear exhibited for glass-metal friction was ductile deformation of the metal, including material removal from the metal and deposition on the glass surface. The amount of observable wear was greatest for dry conditions on smooth substrates. This is because these samples experienced the greatest friction of any experimental conditions due to the lack of water to assist in chemical bond breakage at the glass surface. This produced the greatest shear stress on the steel surface and the most significant wear tracks.
4. Glass composition effects were weaker than roughness or humidity effects. Soda-lime silicate glass exhibited a lower coefficient of friction than either

aluminosilicate or borosilicate glasses for most test conditions, likely due to its greater susceptibility to aqueous attack and its lower hardness when compared with aluminosilicate and borosilicate glasses.

5. Electropolishing alters the topography of metal surfaces in a manner that is highly consequential for frictional mechanics, but which is insufficiently quantified by classical measures of surface roughness. Conventional surface roughness metrics measure surfaces over longer length scales than those that may be relevant for frictional processes, particularly when adsorbed liquid films are involved. Since adsorbed liquid films have thicknesses on the nanometer scale, surface topography at these length scales is most relevant to contact and friction mechanics.

VII. FUTURE WORK

There are many potential avenues to expand on this work. First and foremost, there are multiple opportunities for refinement of the experimental apparatus and methods:

While the surface preparation techniques utilized in this experiment were largely effective at removing organic contamination from the glass surface, surface roughness measurements suggested that there was some residual material on the surface of the glass even after the surface preparation treatment. This residue appears to be remnants of the protective film that the glass was packaged in, and the processes used for surface preparation did not remove all traces of the film from the glass surface. A more aggressive method for removal of the residual material could be employed, such as usage of a cleaning agent prior to thermal treatment.

One of the most crucial limitations of the technique used in this work is that the shapes and sizes of the substrates dictate the test behavior: for flat substrates with minimum dimensions of 25 mm or greater the friction measured is an average of the conditions existing across the entirety of the asperity contacts between the two samples. Furthermore, this contact area is susceptible to variations in sample flatness, and as a result the "real" contact may occur over a very small fraction of the sample, and that location may not move completely in line with the direction of the sample motion. To address this limitation, it may be beneficial to pursue similar work in the with instrumentation and specimens that enable significantly smaller contact areas, perhaps via rods or cylindrical specimens that enable maintenance of a more consistent contact area. The benefits of this are twofold: It is much easier to thoroughly characterize a small, known contact area than a larger area where the actual points of contact and uncertain, and it is simpler to create a uniform surface condition for testing over a smaller area. These changes could enable much tighter correlation of surface conditions to friction results, although the surface geometry would result in an increased force per unit area, and hence a reduction in sensitivity to certain adhesive mechanisms.

An additional step to further improve the quality of measurement would include utilizing a system with greater mechanical rigidity to quicken the response of stick-slip

behavior compared to the relative elasticity of the system used for this work. Minimizing the duration associated with stick/slip events on the data would give a better representation of the dynamic coefficient of friction between the specimens.

Alternatively, one could leverage a different aspect of this experiment as a means for examining friction in other ways, depending on the objective of the study. Specifically, this work showed that deliberate roughening of samples yielded a tighter distribution with lower sample-to-sample variability because smooth-on-smooth interactions are more sensitive to surface flatness and other local geometric variation. Controlled, systematic roughening of glass surfaces might be one method of reducing sample-to-sample variability and thereby minimizing the number of samples required to attain a high-confidence measurement when investigating roughness-independent factors such as glass composition.

There are also straightforward ways of fabricating a much more precise and controllable setup for the humidification apparatus used in this experiment: pass dry air through a known length of water-permeable tubing, and couple this with a temperature-controlled water source to modulate the vapor pressure of the water. Details and performance curves for this type of tubing are available from vendors,[39] and this methodology could be used control humidity both more precisely and over a wider range, thereby enabling more thorough exploration of the friction-humidity relationships examined in this work.

With a more capable experimental setup, there are several opportunities for expanding on the concepts touched on in this work, or exploring them with greater detail and precision.

By more precisely controlling the environmental humidity and hence the extent of adsorbed water on the glass surface, it should be possible to determine more precisely the humidity levels at which the behaviors of different degrees of surface roughness begin to diverge. It is probable that differing surface finishes would exhibit distinctly different friction-humidity curves.

Other authors have found that electropolishing has the side effect of leaving a stainless steel slightly enriched in Chromium relative to a non-electropolished surface.[40] The contribution of subtle differences in steel surface chemistry to glass-steel friction is

largely unexplored, and utilizing different grades of stainless steel of a controlled surface finish would afford an opportunity to assess whether these compositional differences have a significant impact on frictional behavior of steel with glass.

Additionally, microscopy of the stainless steel samples revealed material removal and apparent ductile deformation of stainless steel surfaces. The susceptibility of a particular stainless steel sample to this mechanism could play a major role in its frictional behavior. There are a wide range of stainless steel products that are commercially available, and these include steels over a range of hardness and yield strengths resulting from variations in both metal composition and manufacturing processes. Given the nature of the interactions observed in this work, the impact of variation in the mechanical properties of stainless steel on both the measured coefficient friction and the extent and nature of wear during the friction event would be an interesting area to investigate.

Similarly, the effects of further variations of the glass specimen could be examined. Both soda-lime and aluminosilicate glasses can be chemically strengthened, which has the dual effects of changing the chemical composition at the surface by replacing sodium with potassium, as well as altering the mechanical properties of the glass via the strengthened, compressive layer near the glass surface. Investigation of strengthened glasses could provide some indication on the relative significance of materials' susceptibility or resistance to stress corrosion mechanisms as a friction-influencing property, or whether changes in chemical durability as a function of alkali exchange have a meaningful impact on frictional properties.

This work only briefly touched on wear and its resulting impacts. This work largely attempted to avoid such effects by only measuring friction over short differences and repeatedly using fresh, clean samples to avoid wear effects. Nonetheless, there were measurable trends in friction as a function of test length. Repeating the same study or a subset of it but explicitly focusing on wear effects by using longer test lengths or repeatedly testing specimens would yield additional, interesting data. If previous studies are any indication, it is probable that samples would have significantly different frictional behavior than the pristine surfaces tested over the course of this experimental work. Indeed, it is probable that the results would be substantially different, as after long test durations friction will have altered the surface conditions of the test specimens to such an

extent that the initial surface finish will be secondary to the materials and environment themselves.

VIII. REFERENCES

1. J. Gao, W. D. Luedtke, D. Gourdon, M. Ruths, J. N. Israelachvili, and U. Landman. "Frictional Forces and Amontons' Law: From the Molecular to the Macroscopic Scale," *J. Phys. Chem. B,* **108** [11] 3410-25 (2004).

2. B. N. J. Persson, I. M. Sivebæk, V. N. Samoilov, K. Zhao, A. I. Volokitin, and Z. Zhang. "On the Origin of Amonton's Friction Law," *J. Phys: Condens. Mat.*, **20** [39] 395006 (2008).

3. D. Tabor. "Friction—the Present State of our Understanding," *J. Lubr. Technol.*, **103** [2] 169-79 (1981).

4. K. C. Ludema. *Friction, Wear, Lubrication: A Textbook in Tribology*; p. 78. CRC Press, Boca Raton, FL, 1996.

5. R. Jones, H. M. Pollock, J. A. Cleaver, and C.S. Hodges. "Forces Between Glass and Silicon Surfaces in Air Studied by AFM: Effects of Relative Humidity, Particle Size, Roughness, and Surface Treatment," *Langmuir*, **18** [21] 8045-55 (2002).

6. J. C. Rolf. "Environmental Influences on the Friction Behavior of Glasses"; Ph.D. Thesis, Alfred University, Alfred, NY, 1998.

7. K. L. Johnson. "One Hundred Years of Hertz Contact," *P. I. Mech. Eng.*, **196** [1] 363-78 (1982).

8. B. N. Persson. "Contact Mechanics for Randomly Rough Surfaces," *Surf. Sci. Rep.*, **61** [4] 201-27 (2006).

9. J. A. Greenwood and J. P. Williamson. "Contact of Nominally Flat Surfaces," *Proc. R. Soc. Lond. A*, **295** [1442] 300-19 (1966).

10. A.W. Bush, R.D. Gibson, and T.R. Thomas. "The Elastic Contact of a Rough Surface," *Wear*, **35** [1] 87-111 (1975).

11. K. L. Johnson, K. Kendall, and A. D. Roberts. "Surface Energy and the Contact of Elastic Solids," *Proc. R. Soc. Lond. A*, **324** [1558] 301-13 (1971).

12. R. J. Good and L. A. Girifalco. "A Theory for Estimation of Surface and Interfacial Energies. III. Estimation of Surface Energies of Solids from Contact Angle Data," *J. Phys. Chem.*, **64** [5] 561-5 (1960).

13. P. A. Butz. "Determination of the Static Coefficient of Friction and its Mechanism on the Surface of Soda-Lime-Silicate Glass"; B.S. Thesis. Alfred University, Alfred, NY, 1981.

14. S. Jenkins. "Frictive Behavior of Soda-Lime-Silica Glass"; M.S. Thesis. Alfred University, Alfred, NY, 1986.

15. M. Cummings, Corning Incorporated, Corning, NY, June 2015, Private Communication.

16. A. S. D'Souza and C. G. Pantano. "Hydroxylation and Dehydroxylation Behavior of Silica Glass Fracture Surfaces," *J. Am. Ceram. Soc.*, **85** [6] 1499-1504 (2002).

17. D. B. Asay, and S. H. Kim. "Evolution of the Adsorbed Water Layer Structure on Silicon Oxide at Room Temperature," *J. Phys. Chem. B*, **109** [35] 16760-3 (2005).

18. Z. A. Subhi, K. Fukuda, T. Morita, and J. Sugimura. "Quantitative Estimation of Adsorbed Water Layer on Austenitic Stainless Steel," *Tribology Online*, **10** [5] 314-9 (2015).

19. I. R. McHaffie and S. Lenher. "CCVIII.—The Adsorption of Water from the Gas Phase on Plane Surfaces of Glass and Platinum," *J. Chem. Soc., Trans.*, **127** 1559-72 (1925).

20. J. S. McFarlane and D. Tabor. "Adhesion of Solids and the Effect of Surface Films," *Proc. R. Soc. Lond. A*, **202** [1069] 224-43 (1950).

21. H. He, L. Qian, C. Pantano, and S. Kim. "Effects of Humidity and Counter-Surface on Tribochemical Wear of Soda-Lime-Silica Glass," *Wear*, **342** 100–6 (2015).

22. H. He, L. Qian, C. Pantano, and S. Kim. "Mechanochemical Wear of Soda Lime Glass in Humid Environments," *J. Am. Ceram. Soc*., **97** [7] 2061–8 (2014).

23. G. Stachowiak and A. W. Batchelor. *Engineering Tribology*. pp. 577-616. Butterworth-Heinemann, Oxford, 2014.

24. D. Godfrey and J. M. Bailey. "Coefficient of Friction and Damage to Contact Area During the Early Stages of Fretting I: Glass, Copper, or Steel Against Copper," Technical Note 3011, National Advisory Committee for Aeronautics, Lewis Flight Propulsion Laboratory, Cleveland, OH, September 1953.

25. B. Bhushan, K. Koch, and Y. C. Jung. "Nanostructures for Superhydrophobicity and Low Adhesion," *Soft Matter*, **4** [9] 1799-1804 (2008).

26. J. S. McFarlane and D. Tabor. "Relation Between Friction and Adhesion," *Proc. R. Soc. Lond. A*, **202** [1069] 244-53 (1950).

27. N. Belkhir, T. Aliouane, and D. Bouzid. “Correlation Between Contact Surface and Friction During the Optical Glass Polishing,” *Appl. Surf. Sci.*, **288** 208-14 (2014).

28. J. Meyer, R. Fuchs, T. Staedler, and X. Jiang. “Effect of Surface Roughness on Sliding Friction of Micron-sized Glass Beads,” *Friction*, **2** [3] 255-63 (2014).

29. G. A. Garzino-Demo and F. L. Lama. “Friction and Wear of Metallic and Non-Metallic Surfaces,” *Surf. Coat. Technol.*, **76,** 487-93 (1995).

30. M. L. Rahaman, L. Zhang, M. Liu, and W. Liu. “Surface Roughness Effect on the Friction and Wear of Bulk Metallic Glasses,” *Wear*, **332,** 1231-7 (2015).

31. M. Kalin and S. Jahanmir. “Influence of Roughness on Wear Transition in Glass-Infiltrated Alumina,” *Wear*, **255** [1-6] 669-76 (2003).

32. B. W. Yates and A. M. Duffy. “Statistical Analysis of the Metrological Properties of Float Glass,” 70770D, pp. 1-11 in *Advances in X-Ray/EUV Optics and Components III*, Vol. 7077, Proceedings of SPIE. Edited by A. M. Khounsary, C. Morawe, and S. Goto. SPIE, the International Society for Optics and Photonics, San Diego, CA, 2008.

33. N. Belkhir, D. Bouzid, and V. Herold. “Correlation Between the Surface Quality and the Abrasive Grains Wear in Optical Glass Lapping,” *Tribol. Int.*, **40** [3] 498-502 (2007).

34. Wilsons Ltd, “Stainless Steel – Surface Finishes and Polishing” (2018) Accessed on: June 2018. Available at <http://www.wilsonsmetals.com/datasheets/Wilsons-Ltd_Stainless-Steel-Surface-Finishes--Polishing_135.pdf.ashx>

35. Euro Inox Ltd, “Electropolishing Stainless Steels” (2010) Accessed on: June 2018. Available at <http://www.worldstainless.org/Files/issf/non-image-files/PDF/Euro_Inox/Electropolishing_EN.pdf>

36. “Standard Test Method for Static and Kinetic Coefficients of Friction of Plastic Film and Sheeting”. ASTM Designation D1894-14. American Society for Testing and Materials, West Conshohocken, PA.

37. J. B. Wachtman, W. R. Cannon, and M. J. Matthewson. *Mechanical Properties of Ceramics*. pp. 156-8. John Wiley & Sons, Hoboken, NJ, 2009.

38. C. Ronchetti and G. Salerno. “Structural Glass Lifetime Prediction Model Based on Environmental Variables,” *COST Action TU0905, Mid-term Conference on Structural Glass, Poreč,* 205-14 (2013).

39. Perma Pure, LLC. "FC^{TM}-Series Gas Humidifiers" (2018) Accessed on: July 2018. Available at <https://www.permapure.com/products/gas-humidification/fc-series-humidifiers/>

40. M. Seo and N. Sato. "Surface Characterization of Stainless Steels Prepared with Various Surface Treatments," *T. Jpn. I. Met.*, **21** [12] 805-10 (1980).